

## Durham Research Online

---

### Deposited in DRO:

12 May 2020

### Version of attached file:

Accepted Version

### Peer-review status of attached file:

Peer-reviewed

### Citation for published item:

Tarlatti, S. and Benetti, S. and Callard, S.L. and Ó Cofaigh, C. and Dunlop, P. and Georgiopoulou, A. and Edwards, R. and Van Landeghem, K. and Saher, M. and Chiverrell, R. and Fabel, D. and Moreton, S. and Morgan, S. and Clark, C.D. (2020) 'Final deglaciation of the Malin Sea through meltwater release and calving events.', *Scottish journal of geology*, 56 (2). pp. 117-133.

### Further information on publisher's website:

<https://doi.org/10.1144/sjg2019-010>

### Publisher's copyright statement:

Scottish journal of geology 2020. <https://doi.org/10.1144/sjg2019-010>. © Geological Society of London 2020.

### Additional information:

---

### Use policy

The full-text may be used and/or reproduced, and given to third parties in any format or medium, without prior permission or charge, for personal research or study, educational, or not-for-profit purposes provided that:

- a full bibliographic reference is made to the original source
- a [link](#) is made to the metadata record in DRO
- the full-text is not changed in any way

The full-text must not be sold in any format or medium without the formal permission of the copyright holders.

Please consult the [full DRO policy](#) for further details.

Accepted Manuscript

# *Scottish Journal of Geology*

## Final deglaciation of the Malin Sea through meltwater release and calving events

Serena Tarlati, S. Benetti, S.L. Callard, C. Ó Cofaigh, P. Dunlop, A. Georgiopoulou, R. Edwards, K.J.J. Van Landeghem, M. Saher, R. Chiverrell, D. Fabel, S. Moreton, S. Morgan & C.D. Clark

DOI: <https://doi.org/10.1144/sjg2019-010>

This article is part of the Early Career Research collection available at:  
<https://www.lyellcollection.org/cc/SJG-early-career-research>

Received 18 March 2019

Revised 1 March 2020

Accepted 30 March 2020

© 2020 The Author(s). Published by The Geological Society of London for EGS and GSG. All rights reserved. For permissions: <http://www.geolsoc.org.uk/permissions>. Publishing disclaimer: [www.geolsoc.org.uk/pub\\_ethics](http://www.geolsoc.org.uk/pub_ethics)

When citing this article please include the DOI provided above.

### **Manuscript version: Accepted Manuscript**

This is a PDF of an unedited manuscript that has been accepted for publication. The manuscript will undergo copyediting, typesetting and correction before it is published in its final form. Please note that during the production process errors may be discovered which could affect the content, and all legal disclaimers that apply to the journal pertain.

Although reasonable efforts have been made to obtain all necessary permissions from third parties to include their copyrighted content within this article, their full citation and copyright line may not be present in this Accepted Manuscript version. Before using any content from this article, please refer to the Version of Record once published for full citation and copyright details, as permissions may be required.

# Final deglaciation of the Malin Sea through meltwater release and calving events

Abbreviated title: Malin Sea shelf final deglaciation

Serena Tarlati<sup>\*1</sup>, S. Benetti<sup>1</sup>, S.L. Callard<sup>2</sup>, C. Ó Cofaigh<sup>2</sup>, P. Dunlop<sup>1</sup>, A. Georgiopoulou<sup>3</sup>, R. Edwards<sup>4</sup>, K.J.J. Van Landeghem<sup>5</sup>, M. Saher<sup>5</sup>, R. Chiverrell<sup>6</sup>, D. Fabel<sup>7</sup>, S. Moreton<sup>8</sup>, S. Morgan<sup>9</sup>, C.D. Clark<sup>10</sup>

<sup>1</sup> School of Geography and Environmental Sciences, Ulster University, Coleraine, UK

<sup>2</sup> Department of Geography, Durham University, UK

<sup>3</sup> School of Environment and Technology, University of Brighton, UK

<sup>4</sup> School of Natural Sciences, Trinity College Dublin, Ireland

<sup>5</sup> School of Ocean Science, Bangor University, UK

<sup>6</sup> School of Environmental Sciences, University of Liverpool, UK

<sup>7</sup> Scottish Universities Environmental Research Centre, UK

<sup>8</sup> Natural Environment Research Council, Radiocarbon Facility, East Kilbride, UK

<sup>9</sup> University of Leicester, UK

<sup>10</sup> Department of Geography, University of Sheffield, UK

<sup>\*</sup>Tarlati-S@ulster.ac.uk

## Abstract

During the last glacial maximum, the British-Irish Ice Sheet (BIIS) extended to the shelf edge in the Malin Sea between Ireland and Scotland, delivering sediments to the Donegal Barra Fan (DBF). Analysis of well-preserved, glacially-derived sediment in the DBF provides new insights on the character of the BIIS final deglaciation and paleoenvironmental conditions at the Younger Dryas (YD). Chaotic/laminated muds, ice-rafted debris (IRD)-rich layers and laminated sand-mud

couplets are interpreted as respectively mass transport deposits, plumites and turbidites of BIIS-transported sediments. Peaks in IRD, constrained by radiocarbon dating to after 18 ka cal. BP, indicate discrete intervals of iceberg calving during the last stages of deglaciation. Glacially-derived sedimentation on the slope occurred until ~16.9 ka cal. BP. This is interpreted as the last time the ice sheet was present onto the shelf, allowing glacial meltwater to reach the fan. Bioturbated and foraminifera-rich muds above glaciomarine sediments are interpreted as interglacial hemipelagites and contourites, with the presence of *Zoophycos* suggesting restoration of bottom currents at the transition between stadial and interstadial conditions. During the YD, *Neogloboquadrina pachyderma* sinistral abundances and an isolated peak in IRD indicate the temporary restoration of cold conditions and the presence of icebergs in the region.

**Keywords:** deglaciation, marine terminating ice sheet, ice rafted debris, meltwater, plumites, Younger Dryas

The North-east Atlantic continental margin has been classified into three sedimentary settings: glaciated, glacially-influenced and non-glaciated margin in relation to the contribution of different depositional processes. These processes have produced, since the Pliocene, distinct geomorphologies, including glaciogenic fans, complex canyon systems, mass transport complexes and large contouritic drifts (Stoker 1995; Holmes et al. 1998; Weaver et al. 2000; Piper 2005; Sejrup et al. 2005; Stoker et al. 2005; Sacchetti et al. 2012a). North of 56°N along the glaciated margin, glaciogenic fans, large sediment depocentres built during glacial periods by downslope mass wasting, are the main sedimentary feature (Howe 1995; Armishaw et al. 1998; Howe et al. 1998; Weaver et al. 2000; Sejrup et al. 2005; Stoker et al. 2005). The Donegal-Barra Fan (DBF), located north-west of the island of Ireland (Fig. 1), was formed during Pleistocene glaciations (Stoker 1995) and represents the largest fan associated with the western British Irish Ice Sheet



(BIIS) (Stoker 1995; Clark et al. 2012). Studies in similar settings, along the Norwegian, Arctic, Antarctic and Canadian margins, have shown that glaciogenic fans are more likely to contain a better preserved record of glacially-derived sediments compared to glacial deposits from shallower water and therefore are better suited for the investigation of the dynamics of marine-terminating ice sheets (Lucchi et al. 2015). Data about the timing and character of ice sheet advance and retreat can provide important constraints for ice sheet models to be used to predict the behaviour of modern ice sheets under changing environmental and climatic conditions (Clark et al., 2012).

Although recent glaciological reconstructions focussed on the deglaciation of the BIIS as recorded on the Malin Sea shelf (Callard et al., 2018), and DBF deposits were previously studied in relation to the long-term glacial history the western BIIS (Knutz et al. 2001; Wilson et al. 2002), three sediment cores (6 to 7 m long) collected in 2014 from the DBF as part of the BRITICE-CHRONO project can allow for a more refined interpretation of the regional deglaciation of the BIIS in the Malin Sea, between Ireland and Scotland. The aim of this paper is therefore two-fold: 1) to describe and chronologically constrain the deglaciation of the western margin of the BIIS and 2) to reconstruct the changing environmental conditions in this region from the last glacial to the present interglacial period.

## **Regional setting**

### ***The British-Irish Ice Sheet on the Malin Sea shelf***

The BIIS was a largely marine-terminating and highly dynamic ice sheet that covered most of Ireland and Britain during its maximum extent (Scourse et al. 2009; Clark et al. 2012; Peters et al. 2015). Several phases of advance and retreat on the continental shelf during the last glacial period have been inferred on geomorphological and sedimentological evidence (Van Landeghem et al. 2009; Chiverrell & Thomas 2010; Dunlop et al. 2010; Ó Cofaigh et al. 2012). The BIIS reached its maximum extent on the outer Malin Sea shelf (MSs) at 26.7 ka, followed by a stepped retreat and periods of still-stand marked by grounding-zone wedges identified on the continental shelf (Callard

et al. 2018). Oscillations of the BIIS at millennial scale have been identified from deep-water sediments and seem to correspond with the Dansgaard–Oeschger (D-O) multimillennial climatic cycles recorded in the Greenland ice cores (Knutz et al. 2001; Wilson et al. 2002; Peck et al. 2006; Scourse et al. 2009; Hibbert et al., 2010). On the MSs, numerous glacial landforms (i.e. moraines, drumlins, iceberg scours and lineations) have been mapped and related to the dynamics of the last western BIIS (Benetti et al. 2010; Howe et al. 2012; Ó Cofaigh et al. 2012; Dove et al. 2015). These features suggest the presence of ice streaming offshore from multiples origins in north-west Ireland and western Scotland (North Channel Ice Stream - NCIS, Hebrides Ice Stream - HIS in Fig. 1), before converging on the Malin Sea shelf and delivering large amounts of meltwater and sediment to the DBF. The HIS alone was calculated as draining between 5-10 % of the former BIIS (Dove et al. 2015). Glacial processes therefore transported glaciogenic sediment to the shelf edge and the upper slope of the DBF during periods of ice sheet maximum extent across the shelf and during deglaciation (Knutz et al. 2001; Wilson et al. 2002; Dove et al. 2015; Ballantyne & Ó Cofaigh 2017). The BIIS retreated from the Malin Sea shelf edge around 25.9 ka BP, with most of the continental shelf free of grounded ice at 23.2 ka BP and glacimarine conditions recognised on the shelf up to 20.2 ka BP (Callard et al., 2018). Cosmogenic exposure ages constrained in Western Scotland indicate that ice retreated entirely to the coastline sometime after 16 ka cal. BP (Small et al. 2016; Small et al. 2017).

### ***The Donegal-Barra Fan***

On the continental slope between Scotland and Ireland, the upper part of the Upper Palaeogene to Quaternary sedimentary succession is referred to as the MacLeod sequence and it records the final seaward progradation of the margin through slope-front glaciogenic debris-flows (Stoker et al. 1994; Stoker et al. 2005). The Donegal-Barra Fan (DBF), between 57° N and 55° N along the North East Atlantic margin, is part of this sequence and started forming during the Plio-Pleistocene (Fig. 1; Stoker 1995; Armishaw et al. 1998). The DBF extends from the shelf edge at ca 200 m water

depth to about 2000 m, near the Hebrides Seamount and along the eastern flank of the Rockall Trough (Fig. 1; Ó Cofaigh et al. 2012; Sacchetti et al. 2012b). The fan is a composite glaciogenic fan, generated by the accumulation of numerous sediment lobes (Armishaw et al. 1998; Holmes et al. 1998). It is a complex fan formed by the combination of the Barra Fan, extending mostly north of the Hebrides Seamount and the Donegal Fan, south of it (Armishaw et al. 1998). The sediment lobes, extending up to 250 km in length, are the result of episodes of large-scale downslope mass wasting related to ice streaming across the Malin Sea shelf during glacial intervals (Knutz et al. 2002; Sacchetti et al. 2012a). The fan has been described as the largest sedimentary body resulting from the drainage of the western BIIS, occupying an area of 6300 km<sup>2</sup> and with a maximum thickness between 400 and 700 m (Armishaw et al. 1998).

### ***Regional oceanography***

Several currents contribute to the winnowing of sediments and the deposition of contourites on the North-east Atlantic continental margin including the DBF region (Faugères et al. 1981; Howe 1996; Howe et al. 1998; Stoker 1997; Knutz et al. 2002; Masson et al. 2010; Georgiopoulou et al. 2012). The main surface current in the North Atlantic is the North Atlantic Current (NAC). The Eastern North Atlantic Water (ENAW) originates from the NAC in the Bay of Biscay and is observed at ca. 1000-1500 m water depth on the eastern side of the Rockall Trough (Fig. 1 inset). It turns anticlockwise along the Hebrides Seamount and then moves south along the western margin of the trough (Holliday et al. 2000; Read 2000). It is advected northward by the Shelf Edge Current (SEC) with an average speed of 15-30 cm/s (New & Smythe-Wright 2001). In the deeper part of the basin and driven by the Deep Northern Boundary Current (DNBC), the North Atlantic Deep Water (NADW) flows along the lower continental slope and within the trough between 2 and 3 km water depth (Fig. 1 inset; McCartney 1992; Dickson & Kidd 1987). During Quaternary glaciations, the release of large amounts of freshwater from ice sheets had a fundamental role on the deceleration or interruption of Atlantic oceanic currents (Stanford et al. 2011; Bigg et al. 2012; Toucanne et al.

2015). Many studies show that these oceanographic changes, as well as the restoration of typical interglacial oceanographic conditions following deglaciation, can be recorded in the North Atlantic sediments (among others Rahmstorf 2002; McManus et al. 2004; Austin & Kroon 2001).

## Materials and methods

The three sediment cores analysed in this study were collected as part of the larger BRITICE-CHRONO project in 2014 by piston coring during cruise JC106 on the *RRS James Cook* (Table 1; Fig. 1). The cruise collected around 220 cores all around Ireland in shallow and deep water to investigate the last BISS glacial maximum extent and retreat. The specific cores that are used in this study targeted the DBF (Fig. 1). Sites were picked using acoustic data collected with a hull-mounted Kongsberg SBP120 sub-bottom profiler, chirp system operating with a sweep frequency of 2.5 kHz to 6.5 kHz, with a depth resolution of 0.3 ms. Core sites were selected on the slope between water depths of 1036 m and 1537 m, where there was little evidence of reworking by bottom currents and avoiding large escarpments. The sub-bottom data were imported into IHS Kingdom as 2D survey lines for visualisation and processing. These are used in this paper to provide a broader stratigraphic context for the cores. Acoustic units were identified following the methodology outlined in Mitchum et al. (1977) and the depth and thickness in two-way travel time (tw-t-ms) of the units was converted using the average P-wave velocity acquired by multi sensor core logging of the recovered cores before splitting ( $1500 \text{ ms}^{-1}$ ; relevant core logs are reported in Tarlati, 2018). In this study, only one profile crossing the locations of JC106-134PC and JC106-133PC is used (Fig. 2).

Cores have a recovery between 661 and 672 cm (Fig. 1; Table 1) and were analysed, soon after collection, with a Geotek Multi-Sensor Core Logger (MSCL) at 2 cm intervals for physical properties. Each core was split, photographed and visually described. X-radiographs were acquired using a CARESTREAM DRX-Evolution System. X-radiographs were used to identify sedimentary structures not visible to the naked eye (cf. Howe 1995). Grain size analyses were carried out using a

MALVERN Mastersizer 3000. Samples were collected ca. every 20 cm along core. Each sample was between few milligrams and few grams in weight according to grain size in order to achieve optimal obscuration in the Mastersizer. Samples were soaked in a 50 ml 5% Calgon concentrated solution, then placed on a shaking table overnight to guarantee the disintegration of flocculated particles. The results are reported in mean volume weight values  $D(4;3)$  (cf. Mingard et al. 2009). X-radiographs, magnetic susceptibility (MS) and grain size distributions were used to aid lithofacies identification and interpretation of their depositional processes.

Planktonic foraminifera and IRD counts were conducted in the fraction coarser than 150  $\mu\text{m}$ , on 1 cm thick slabs collected separately from grain size samples at a 20 cm intervals downcore and wet-washed with a 63  $\mu\text{m}$  sieve. The counting included at least 300 specimens for the planktonic foraminifera and a minimum of 300 lithic grains, when recognised, for the IRD. IRD counts were carried out on a total of 106 samples across the 3 cores. IRD concentration [IRD] was calculated as the number of lithic grains on the total dry sediment weight (cf. Haapaniemi et al. 2010; Peck et al. 2006; Scourse et al. 2009). Calculation of the abundance for the polar species *Neogloboquadrina pachyderma* sinistral (NPS) was conducted with the aim of identifying colder stadial intervals (Bond et al 1993). Foraminifera counts were conducted on the same 36 samples that were used for IRD counts and only in core JC106-133PC. This core was selected for the NPS analysis based on preliminary visual description as it shows the most diverse sediment record of the three. It is also the core furthest away from the former ice margin and therefore, it is assumed that it represents a more open-water environment, likely to record regional climatic and oceanographic changes, in addition to BIIS related proglacial processes.

A total of seven Accelerator Mass Spectrometer (AMS) radiocarbon dates using monospecific planktonic foraminifera, or mixed benthic foraminifera were acquired for this study (Table 2). The samples typically targeted lithofacies boundaries or distinct peaks in the IRD content, avoiding areas with signs of erosion and bioturbation. The dated samples were then calibrated using OxCal 4.2 (Ramsey 2009) with the Marine13.14c calibration curve (Reimer et al. 2013) which has an

inbuilt 400-year marine reservoir correction. Table 2 presents the radiocarbon and calibrated dates, with three separate age simulations using  $\Delta R$  values of 0, 300 and 700 years to account for uncertainty over the spatial and temporal variation in the marine reservoir effect in the North Atlantic and adjoining continental shelves since the Last Glacial Maximum (e.g. Wanamaker et al. 2012). For ease of presentation, only the calibrated ages with a  $\Delta R$  of 0 years are used to describe the timing of events in the text. This protocol for reporting radiocarbon ages was agreed among the members of the BRITICE-CHRONO Consortium to allow for an easier comparison of results across the different transects. One sample was rejected from the age reconstruction because it was found to be collected in an interval later recognised as a gravity flow deposit (turbidite), sample 133PC 375-376 cm.

Radiocarbon dates have been used to assess the age range for the sediments. Additionally, the presence of peaks or distinct intervals of consistently high values of IRD and NPS concentrations for core JC106-133PC were used to support the identification of stadial and interstadial intervals in the sediment record, together with the radiocarbon dates. NPS% commonly indicates changes in sea-surface temperature and it represents the most abundant polar species during cold intervals such as Marine Isotope Stage 2 (MIS2; Bond et al. 1993). In this region, NPS% has been observed to have a direct correlation with both the trends in IRD delivery from BIIS and air temperature changes recorded in ice masses, with peaks in NPS% being in tune with stadials in the Greenland oxygen isotope record (Peck et al. 2006; Peck et al. 2007; Haapaniemi et al. 2010; Rasmussen et al. 2014). As in core JC106-133PC, the NPS% shows a direct correlation with the IRD concentration (Fig. 4), for the interpretation of the chronostratigraphy of all cores, the [IRD] is also considered a good approximation for NPS%. When possible, based on the assessed chronostratigraphy, sedimentation rates were calculated for some of the lithofacies, with the interpreted mass transport deposits and turbidites excluded from the calculations (cf. Benetti 2006).

## Results

## *Acoustic data*

### Description

Five acoustic units and local escarpments are identified in the seismic profile (Fig. 2). Acoustic units are not always laterally continuous along the full length of the slope due to the presence of the escarpments, but they are classified based on their similar internal seismic character when identified in different sections of the slope. The maximum seismic signal penetration is 35 m. High amplitudes are observed between 30 and 10 mbsf, with thinner low amplitude or transparent seismic units above them. Escarpments are predominantly found within these units and at different water depths along the slope (ca. 800m, 1110m and 1350-1400m wd). The slope is physiographically subdivided in lower (below 1400 m wd), middle (between 900 and 1400 m wd) and upper (above 900 m wd) based on the slight changes in gradients and presence of distinct escarpments.

Acoustic unit 5 is observed along the middle and lower slope (between 1200 and 1600 m wd, Fig. 2a and 2b). It is a (mostly) transparent acoustic facies with rare sub-parallel low amplitude reflectors. Its upper contact is sharp (Top Unit 5) and its basal boundary is below the depth of seismic signal penetration (Fig. 2a).

Acoustic unit 4 is recognised in all sections of the slope. It is characterised by sub-parallel and continuous reflectors of variable amplitude, with a wavy upper (purple in Fig. 2) boundary. In the lower slope, it contains undulating sub-parallel and continuous reflectors (Fig. 2a), with an overall thickness between 20 and 25 meters. In the middle slope it is thicker, between 30 and 45 m thick, with sub-parallel reflectors showing an asymmetrical aspect and up-slope propagation (Fig. 2b). In the upper slope, it is found deeper than 30 mbsf, with low amplitude and wavy, sub-parallel reflectors (Fig. 2c). A continuous basal boundary is visible along the lower and the middle slope (Fig. 2a, b) but the signal gets lost in the upper slope due to the attenuation with increased depth below the seafloor (Fig. 2c).



Acoustic unit 3 is recognised only along the upper slope (between 900 and 700 m wd) overlaying unit 4, it is acoustically semi-transparent and chaotic. It has a varying thickness between 10 and 30 m, with a continuous low amplitude basal reflector (purple in Fig. 2c) and a discontinuous upper boundary (light blue in Fig. 2c).

Acoustic unit 2 is identified intermittently along the middle and upper slope, directly overlaying unit 4 on the middle slope and unit 3 on the upper slope. It ranges between 5 and 10 m in thickness (Fig. 2b, 2c) and it is internally characterised by low amplitude sub-parallel reflectors. Its upper boundary is represented by a high amplitude, undulated and discontinuous reflector (yellow in Fig. 2b, c). The lower boundary is the light blue low amplitude discontinuous reflector in the upper slope (Fig. 2c), and the high reflectance pink reflector along the middle slope (Fig. 2b).

Acoustic unit 1 is found overlaying unit 4 along the lower slope (Fig. 2a), and unit 2 on the middle and upper slope (Fig. 2b, c). It is the near-seafloor acoustic facies, with a thickness up to ~3 m and is represented by low amplitude sub-parallel reflectors. Its upper boundary is the seabed, which is characterised by a high amplitude, undulated and continuous reflector (dark blue in Fig. 2a, b, c).

On the seabed, a ~6 m high escarpment is recognised at 1095 m water depth (middle slope, Fig. 2b). Two escarpments (between 5 and 15 m high) are visible in the uppermost facies and at the seafloor along the upper slope (Fig. 2c), accounting for some of the discontinuity in the unit. No sediment cores were retrieved from this part of the slope. JC106-133PC was recovered from the lower section of the slope and it sampled acoustic unit 1 and the top part of unit 4 (Fig. 2a); core JC106-134PC was collected from the middle slope (Fig. 2b) and it sampled acoustic units 1 and 2.

### Interpretation

Acoustic data described above, provide a stratigraphic context for the BIIS and DBF paleo environmental reconstruction. The five units identified here show similarities with previously published seismic data for this margin, which identify a stack (up to 60 m thick) of reworked glaciomarine sediments forming the upper MacLeod Sequence (Stoker et al. 1994; Stoker 1995).



Unit 5 with its acoustically transparent character, could represent the debris flow deposits in the lower unit of the upper MacLeod Sequence (Stoker et al., 1993). Both acoustic units 4 and 2, which show continuous, wavy and subparallel reflectors in the lower and middle slope (Figs 2a and 2b), are interpreted as Late Pleistocene glaciomarine sediment deposits. In the middle slope, unit 4 displays upslope-climbing asymmetrical reflectors, (Fig. 2b), which are typical of sedimentary wave migration during intervals of large sedimentary input and high sedimentation rates (Wynn & Stow 2002). Along the upper slope (Fig. 2c) the occurrence of the buried escarpments within these glaciomarine deposits suggest that they were likely also affected by localised down-slope mass movements. Acoustic unit 3 on the upper slope with its chaotic and semi-transparent character (Fig. 2c) is interpreted as debrites, based on its similarity with the Peach Slide deposits mapped at other locations on the Donegal Barra Fan (Owen et al., 2018). Overall, between 30 and ~5 mbsf, the record is interpreted as distal glaciomarine sediments redistributed by mass flow processes such as debris flows and turbidity currents, similarly to what is observed further to the north along the Hebrides slope (Stoker et al. 1994; Stoker 1995; Armishaw et al. 1998; Knutz et al. 2002).

The uppermost acoustic unit 1, along the entire slope above ~3 mbsf, is interpreted as recording Holocene hemipelagic and contouritic deposition as observed elsewhere on the fan, where similar acoustic facies and sediments are identified and dated (Armishaw et al. 1998; Knutz et al. 2002; Owen et al. 2018).

### ***Chrono- and lithostratigraphy***

#### ***Lithofacies description and lithostratigraphy***

Five lithofacies are defined based on lithology, sediment colour, internal sedimentary structures, mean grain size and magnetic susceptibility (Fig. 3-7). They are described in the following sections from core bottom to top and from deeper to shallower water depths.

*Laminated mud rich in IRD (ILM):* This lithofacies is an olive-brown laminated mud rich in IRD. The diameter of the IRD grains, observed on the split ore and X-radiographs, ranges from a few

mm to 5-6 cm and the grains are not equally distributed within the facies. Laminations are not always visible to the naked eye but clearly evident on the X-radiographs (Fig. 3). Bioturbation is not noticeably present and foraminiferal content is low. The mean volume grain size is extremely variable, fluctuating from 10 to 100  $\mu\text{m}$  due to variable IRD content. Magnetic susceptibility ranges between 80 and 200 ( $10^{-5}$  SI) (Fig 4-6). This lithofacies is found in all three piston cores, constitutes most of the sediment record and has a thickness of up to 3.5 m (Figs 4, 5 and 6). Core JC106-133PC, the deepest and most westerly located core (Figs 1 and 4), contains ILM from the core base (660 cm bsf) up to 370 cm down core and again at ca. 185-135 cm down core (Fig. 4). In core JC106-128PC (Figs 1 and 5), ILM represents the dominant lithofacies from the core base to 95 cm core depth. It is observed also as a 5 cm thick interval at 30-35 cm with sharp basal and gradual top contacts. In core JC106-134PC, the more proximal to the shelf edge (Figs 1 and 6), ILM also represents the main lithofacies, extending from the base of the core up to 120 cm down-core.

*Chaotic mud (CM)*: This lithofacies, present in all cores, is an olive-brown, poorly sorted mud, devoid of foraminifera, with well-defined shear surfaces and floating mud clasts (Fig. 3). No primary sedimentary structures are present but rare wispy and dipping laminations are observed (Fig. 3). It has an overall chaotic appearance and is characterised by a large range of MS values (100-300  $10^{-5}$  SI) and a grain size of  $< 20 \mu\text{m}$  in volume weight D(4;3) (Figs 4, 5 and 6). Core JC106-133PC contains one 7-cm thick CM interval is at 275 cm (Fig. 4). In JC106-128PC four CM deposits, bounded by inclined and sharp planes, are identified through the ILM interval at 310 cm, 449 cm, 547 cm and 590 cm downcore, with thicknesses ranging between 5 and 25 cm (Fig. 5). In JC106-134PC a 1 m-thick CM deposit is recognised between 210 cm and 310 cm, with an inclined sharp surface at the top and faint and inclined lamination within it. A 10 cm-thick CM deposit was also recognised at 50 cm bsf (Fig. 6), this unit is wedge shaped and marked by two inclined (up to  $45^\circ$ ) sharp surfaces, bounded with fine silt (Fig. 3).

*Laminated sand to mud couplets (LSM)*: Olive-brown laminated sand to mud couplets, with laminated basal sand and sharp basal contacts are observed in all cores, mostly on the X-

radiographs. Each unit of this lithofacies include multiple fining upward couplets with a coarser sand base gradually fining into mud (Fig. 3). Ripples are recognised within the sandy interval, bioturbation is absent and foraminifera are scarce. Generally, the couplets are between 5-10 cm thick and the facies is marked by high magnetic susceptibility, with values between 160 and 270 ( $10^{-5}$  SI) (Figs 4, 5 and 6). In core JC106-133PC three intervals of LSM, with thicknesses varying between a few cm to 7-8 cm, were identified around 380 cm, 390 cm and 444 cm down core, highlighted by increased MS values, reaching over 200 ( $10^{-5}$  SI) (Fig. 4). In JC106-128PC a LSM interval at 182 cm core depth displays a sharp basal contact and a thickness of 8 cm, it is identifiable by a peak in MS reaching 160 ( $10^{-5}$  SI) (Fig. 5). In JC106-134PC, LSM is observed at 198-195 cm, it is indicated by an increase in the mean volume grain size and a peak in MS of 200 ( $10^{-5}$  SI) (Fig. 6).

*Extensively bioturbated mud (BM):* This lithofacies is a brown mottled sandy mud, rich in foraminifera and extensively bioturbated (Fig. 3), showing an abundant presence of *Zoophycos* burrows. *Zoophycos* is an ichnofacies characterised by long tubular structures parallel and sub-horizontal within the sediment, with a thickness no less than 1 cm (cf. Löwemark et al. 2006). The distribution of this ichnofacies in the JC106 cores varies with core depth. The burrows are abundant at the base of this facies but reduce upward in the sediment record. This facies is found in all three piston cores: at the core tops of JC106-133PC and JC106-134PC, and below the foraminifera-bearing mud lithofacies (FM) at the top of core JC106-128PC (Figs 4, 5 and 6). It is up to 2 m thick and generally darker than FM and lighter in colour from the facies below (ILM). Within this lithofacies both fining and coarsening upward trends in grain size were observed, with both sharp and gradual basal and upper contacts. This facies has a high content of foraminifera and the characteristic grain size is measured between 20 and 40  $\mu\text{m}$  in mean volume weight  $D(4;3)$ . Magnetic susceptibility varies greatly within the facies between 40 and 120 ( $10^{-5}$  SI) (Figs 4, 5 and 6). No primary sedimentary structures are visible. In core JC106-133PC, at 375 cm core depth the sediment record changes upwards gradually over 10 cm into BM, which extends up to 185 cm core

depth; then BM is recognised at 135 cm and continues to the core top (Fig. 4). In core JC106-128PC above 95 cm, ILM gradually passes into BM over a few cm and extends up to 5 cm up core (Fig. 5). In JC106-134PC BM extends with a gradual contact from 120 cm core depth up to the core top (Fig. 6).

*Foraminifera-bearing mud (FM)*: A light brown, sandy foraminiferal mud was recognised only at the top of core JC106-128PC. This facies shows bioturbation, clearly visible in the X-radiographs (Fig. 3). The mean volume grain size is 30–40  $\mu\text{m}$ , with the foraminifera making up the bulk of the coarser fraction. It has a thickness of approximately 5 cm and there is a gradual contact with the darker underlying lithofacies (BM). The acquisition of magnetic susceptibility was not possible for this facies because of its limited thickness and position at the core top.

Overall, the three cores show a similar internal organisation of lithofacies from base to top (Figs 4, 5 and 6), although core JC106-128PC contains a larger number of CM deposits compared with the other two. Generally, the ILM constitutes most of the core sediments in the lower half of the cores. LMS are identified in all three cores within the upper part of ILM close to the transition to BM. Conversely, the CM lithofacies does not display a noticeable trend as these intervals are present throughout the record. BM is characteristic of the upper part of all cores, except for the thin FM at the top of JC106-128PC (Fig. 5). This facies is not present in the other two cores. A separate ILM interval interrupts the BM deposits in the upper parts of JC106-133PC and JC106-128PC, but not in JC106-134PC the shallowest of the cores.

#### *Ice-rafted debris (IRD) concentration and Neogloboquadrina pachyderma abundance*

IRD in all three cores is mainly composed of quartzite, granite and basalt. The lowest [IRD] values are measured at the core tops and within the BM lithofacies. The highest concentrations are observed in ILM, with 6730 grains/g of dry sediment at 350 cm down-core in JC106-134PC (the most proximal core to the shelf edge; Fig. 6).

In core JC106-133PC, [IRD] within the BM is very low, with values close to 0 (Fig. 4). In the ILM, in the bottom half of the core, [IRD] is consistently high, with a minimum of 1000 grains/g and an average of 1656 grains/g per sample (Fig. 4). Two peaks in [IRD] are observed within this interval at 453 and 585 cm with respective values of 2340 and 3600 grains/g. One additional peak in [IRD] is recognised within ILM in the upper part of the core between 140 and 175 cm, with values up to 1428 grains/g. These three peaks are relatively sharp and represent a two- to three-fold increase in IRD concentration compared to the values above and below them.

In core JC106-128PC, the [IRD] shows an irregular pattern, with lowest values (<200 grains/g) in the BM and many peaks throughout the core with maximum values of 2180 and 1910 grains/g (Fig. 5). The highest peaks are recognised within CM, while peaks in the ILM have values of 1030 and 1620 grains/g.

Similarly to JC106-128PC, [IRD] in core JC106-134PC displays a certain variability with the lowest values measured through the BM between 0 and 1000 grains/g (Fig. 6). Generally, higher [IRD] are observed in the ILM, with an average of 1547 grains/g. Two [IRD] peaks within the ILM are recognised at 350 and 550 cm with values up to 6730 and 3026 grains /g.

The abundance of the planktonic foraminifera *Neogloboquadrina pachyderma* sinistral (NPS%) calculated in core JC106-133PC shows an alternation between high and low values (Fig. 4). The NPS% abundance mirrors the IRD curve, with high NPS% corresponding with IRD peaks and characterising the ILM. NPS% is low at the core top, with values <10% of the planktonic foraminifera assemblage between the core top and 120 cm of core depth. Further down the core, a sudden increase between 140 and 195 cm is recorded with NPS%  $\geq 80\%$ . Between 195 cm and 355 cm down-core, the NPS% is reduced again to values <10 %. At 375 cm of core depth, the NPS abundance increases suddenly and significantly, exceeding values of 80%, and remains high in the lower part of the core.

#### Sedimentary facies interpretation and chronostratigraphy

Sedimentological, microfaunal and chronostratigraphic evidence from the three cores allow the interpretation of the sedimentary processes active along the Hebrides Margin and the DBF.

The lithofacies identified in the sediment record are interpreted as corresponding to five different sedimentary processes discussed below (Fig. 7). Based on the available radiocarbon dates and pattern of IRD and NPS distribution compared to other records in the region and their turning with the Greenland oxygen isotope record (cf. Peck et al. 2006; Peck et al. 2007), most of the sediment in the cores appears to be younger than 18 ka cal. BP and therefore time-constrained to Marine Isotopic Stage (MIS) 1 and the latter part of MIS2 (Fig. 7). The only core where the bottom age is more uncertain is JC106-128PC, for which only one radiocarbon date higher up in the core exists; nonetheless the [IRD] trend does not suggest major stratigraphic differences from the other cores.

The laminated mud rich in IRD (ILM) interval at the bottom of all cores is interpreted as a plumite based on the planar laminations, presence of IRD and lack of bioturbation. Plumites are deposited mostly by settling of fine-grained sediments from meltwater plumes, in conjunction with ice-rafted material from icebergs and meltwater plumes have been observed to deliver fine sediment up to 250 km from the basal ice sheet meltout location (cf. Wang & Hesse 1996; Hesse et al. 1997; Dowdeswell et al. 1998; Hesse et al. 1999; Ó Cofaigh & Dowdeswell 2001; Lekens et al. 2005; Lucchi et al. 2002; Prothro et al. 2018). The cores in this study were retrieved at a maximum of 200 km from the inferred closest ice-margin (Finlayson et al. 2014; Small et al. 2017; Callard et al. 2018). The highest IRD concentrations are considered to reflect a relative increase of iceberg discharge during calving events (cf. Andrews 2000; Scourse et al. 2009). Based on the radiocarbon dates, plumite deposition on the DBF was ongoing around 18 ka cal. BP (approximately the bottom of the cores) and continued till around 15.5 ka cal. BP, correlating broadly with the timing of Greenland Stadial 2 (GS-2; 23.3 to 14.7 ka cal. BP). Sedimentation rates calculated using the available radiocarbon dates for the plumites are 166 cm/ka in JC106-134PC (shallowest and closest to the continental shelf break), and 131.8 cm/ka in JC106-133PC (deepest and furthest from the shelf break); whilst it is not possible to assess a sedimentation rate for JC106-128PC due to the lack

of chronological control at the bottom of this core. Plumites are again identified as a distinct layer within the sediment record of the middle and lower slope at the Younger Dryas (YD; Alley 2000) or Greenland stadial 1 (GS-1; 12.9 to 11.5 ka cal. BP).

The fining upward and sedimentary structures, such as ripples and planar laminations, within the sand to mud couplets (LSM) suggest that they were deposited from dilute, low-density turbidity currents; whilst their rhythmic nature and deep water location very likely indicate the origin of such turbidity currents from prolonged bursts of meltwater release from the ice margin (Middleton & Hampton 1976; Lowe 1979; Lowe 1982; Wang & Hesse 1996; Hesse et al. 1997; Hesse et al. 1999). Rhythmic deposits of laminated sand to mud couplets are identified elsewhere along polar and North Atlantic continental margins and they have been used as a proxy for periods of particularly intense meltwater delivery during the last deglaciation in distal locations to the source of the flows (Dowdeswell et al. 1998; Piper and Normark 2009; Roger et al. 2013). On the DBF, they deposited around 17-16 ka cal. BP (Fig. 7) and they are found as thin turbidite intervals within the upper plumite deposits, thus suggesting distinct episodes of more intense glacial meltwater release within overall deglaciation (cf. Callard et al 2018).

Overlying the plumites, the bioturbated mud (BM) is interpreted on the basis of bioturbation and mottling and the lack of primary sedimentary structures (Fig. 7) as contourites (i.e. sediment reworked and winnowed by bottom-currents; Stow 1979; Stow & Lovell 1979; Stow & Piper 1984; Stow et al. 2002; Rebesco et al. 2014). Based on their mean grain size ( $<30\ \mu\text{m}$ ), the contouritic deposits can be classified as muddy contourites (cf. Stow et al. 2002; Rebesco et al. 2014). The *Zoophycos* ichnofacies within the contourites allows for the identification of an initial restoration of the bottom currents and of intermediate climatic conditions in the region. This *ichnofacies* appears to be dominant and is consistent with a well-developed burrowing network in deep-water ecosystems that developed at the transition between cold and warm climatic stages (Dorador et al. 2016). The transition from plumite to *Zoophycos*-dominated contourites occurs in the cores between ~16 and ~15.2 ka cal. BP. Contouritic deposition continues to sometime after 12 ka cal. BP (Fig. 7)



and possibly to modern day as this facies continues to the tops of cores JC106-133PC and JC106-134PC although the tops have not been dated (Fig. 7). If the core tops represent modern day sedimentation, the sedimentation rate since ~ 15 ka cal. BP would be at the most ~3.5 cm/ka for JC106-134PC and ~ 7.8 cm/ka for JC106-128PC. For core JC106-133PC, where the contouritic unit is 360 cm thick but interrupted by a 50-cm thick YD plumite (Fig. 4), sedimentation rate for contouritic sediments would be 21 cm/ka for the same period.

Chaotic mud (CM) intervals occur within the plumite and the contouritic facies (Fig. 7). These intervals are interpreted as mass transport deposits due to slope instability (Holmes et al. 1998; Tripsanas & Piper 2008). The interpretation is supported by the identification of inclined (up to 45°; Fig. 3) sharp contacts inferred as shear surfaces and the presence of mud clasts. Similar deposits have been identified within glaciogenic sediments along other glaciated margins (Aksu & Hiscott 1989; Tripsanas & Piper 2008; Garcia et al. 2011). Their presence throughout the length of the cores suggests that slope instability has occurred on the slope in the last ~18 ka.

The thin (5 cm) interval of foraminifera-bearing mud (FM) at the top of JC106-128PC (highlighted in Fig. 7 by the yellow arrow) is interpreted as a hemipelagite, the result of slow settling of mud and foraminiferal tests in a low energy depositional environment where bioturbation is common (Stow et al. 1996; Stow & Mayall 2000; Howe 1995; Knutz et al. 2001). The hemipelagite is not directly dated but its similarities with other deposits reported in the vicinity, such as characteristic colour, presence of foraminifera and the core top position (along the Irish margin: Howe 1995; Knutz et al. 2002; on the DBF: Howe 1996; Knutz et al. 2001; Wilson et al. 2002; and in the Rockall Trough: Howe 1995; Georgiopoulou et al. 2012) suggest that this facies represents the most recent Holocene deposition. The hemipelagite does not seem to be present in JC106-133PC and JC106-134PC; its absence could be attributed to the presence of erosional bottom currents at specific water depths in the region (cf. Howe 1995; Howe et al. 1998) or coring disturbance resulting in the loss of core tops (cf. Buckley et al. 1994).



Overall the observed lithofacies are all characteristic of sedimentation along a formerly glaciated margin, with plumites constituting the majority of the record and showing that the deposition of fine grained glaciomarine sediments and IRD was dominant along the slope almost to the end of MIS2 and during the YD. Downslope mass movements, recorded as turbidite and debrite deposits, seem to have occurred episodically before the YD. Contourites and occasionally hemipelagites characterise the sedimentary record since 15.5 ka cal BP. All these lithofacies are contained within acoustic units 2 and 1 in the seismic record (Figs 2b and 2c) and their interpretation well matches with the interpretation of such units as distal glaciomarine sediments deposited post last glacial maximum and Holocene contourites and hemipelagites.

## Discussion

### *The Late Quaternary DBF sedimentary record*

The interpretation of the sedimentary processes and their timing reveal how sedimentation in the DBF evolved during the Late Quaternary as the BIIS margin retreated from the Malin Sea shelf edge (Fig. 8). Recent reconstructions of BIIS dynamics suggest that the ice margin around 18-17 ka cal. BP was already located in the inner MSs. Total deglaciation of the MSs and retreat of the ice-limit to the present coastline and consequent interruption of the Hebrides Ice Stream (HIS), has been dated between 17 and 16 ka cal. BP (Dove et al. 2015; Small et al. 2016; Small et al. 2017; Ballantyne & Ó Cofaigh 2017; Callard et al. 2018). The high sedimentation rates in the plumites (160 to 130 cm/ka) on the DBF suggest a large influx of sediment to the area between 18 and 15.5 ka cal. BP. At this time the most likely source of consistent and significant sediment supply would have been iceberg calving and concentrated meltwater plumes from a melting and retreating BIIS along western Scotland and the Hebrides. Glaciomarine sediments younger than 20 ka cal. BP have also been identified on the MSs but cessation of glaciomarine conditions on the shelf has not been dated (Callard et al. 2018). The timing of deposition on plumites on the DBF suggests that meltwater release into the Malin Sea continued to at least 16-15.5 ka cal. BP, thus slightly later than current reconstructions for the BIIS ice margin. Given the closer proximity of the DBF to the Outer

Hebrides (~100km) compared to the rest of the Scottish coastline, it is possible that the plumites recovered in the DBF cores represent the final stages of retreat of the HIS (Hesse et al. 1997; Dove et al. 2015; Small et al. 2017; Prothro et al. 2018).

Following deglaciation, contouritic deposition ensued at ~15.5 ka cal. BP. The presence of the *Zoophycos* ichnofacies in the contourites suggests an increase in temperature and a restoration of bottom current speed following the weakening during MIS2. The decrease in *Zoophycos* burrows toward the core tops can be attributed to an increase in bottom current velocities and temperature through time, representing a transition to modern climatic conditions within the Holocene (cf. Dorador et al. 2016). Such an increase in current speed would have had the potential to winnow the sediments in the study area and may be responsible for the limited thickness of the post-glacial and Holocene sediments in the upper and middle slope. Elsewhere on the DBF and the NE Atlantic slope, sediment winnowing in the Holocene has been attributed to the NADW current, and in particular to the flow of ENAW between 1000 m and 1500 m of water depth (Knutz et al. 2002). The two cores from the upper and middle slope in this study were collected respectively at 1036 m and 1475 m water depth, within the active flow of the ENAW. On the other hand, the lower slope core was collected beyond 1500 m water depth and the contourite thickness (>2.5m) and higher sedimentation rate after 15 ka cal. BP for this location testifies to weaker current activity at this water depth.

Hemipelagite deposition is not particularly prominent along this stretch of the margin demonstrating the switching off of sediment supply and suggesting sediment starvation, as observed elsewhere on current-swept North Atlantic continental slopes (Rashid et al. 2019). Only a thin hemipelagic layer is present at the top of core JC106-128PC on the middle slope. We can only speculate that this hemipelagite represents the most recent sedimentation and that the transition into this different style of sedimentation could be related to further changes in oceanic circulation and/or reduced sediment supply in the study area. However, our data is too limited to discuss this any further.

***IRD peaks and calving events***

Iceberg calving is the most likely process for the delivery of sand and coarse size lithic grains to the core sites (Lekens et al. 2005; Rorvik et al. 2010). Three peaks in IRD are identified and correlated across cores. The two bottom peaks are dated before 16 ka cal. BP: one was directly dated at ~17.8 ka cal. BP, whilst the younger is inferred to have been deposited around ~16.9 ka cal. BP based on the calculated sedimentation rate for plumites. The third IRD peak, only recognized in core JC106-133PC the most distal and deepest of the cores, is directly dated at the YD, ~ 12.7 ka cal. BP. A relatively small increase in [IRD] is also recognized on the middle slope core (JC106-128PC) in the plumite layer within the contourite in the core upper part.

IRD is represented largely by quartzite, basalt and highly metamorphic grains, common components in the Archean to Proterozoic rocks of the North Atlantic, including Western Scotland and north of Ireland (Bailey et al. 2013; Arosio et al. 2018). The same petrologies have been found elsewhere on the DBF and were associated to the BIIS (Knutz et al. 2001). IRD peaks during MIS2 are therefore interpreted as the result of BIIS calving events from the Malin Sea area, also in agreement with the other BIIS reconstructions previously discussed that recognise a retreating ice margin along the shelf and interruption of ice-streaming around 16 cal. ka BP (Dove et al. 2015; Small et al., 2017; Callard et al., 2018). The petrological data do not allow however a distinction between possible Irish or Scottish sources.

The source of the IRD peak deposited at the Younger Dryas is not as straightforward to identify with the data available here. During the YD, ice extent in Ireland appears to have been confined to mountain glaciers that did not extend to sea-level, but the ice cap in Scotland had several active tidewater glaciers that could have possibly been the source of icebergs in the Malin Sea (Ballantyne et al. 2008; Scourse et al. 2009). However, sediment reworking resulting in a mix of YD and older sediments and intense iceberg scouring at the shelf edge, and lack of thereof in the middle and inner shelf (Benetti et al. 2010; Dunlop et al. 2010; Ó Cofaigh et al. 2012; Callard et al. 2018), suggest that icebergs that crossed the region at the time were more likely coming from the outer ocean,

instead of the Scottish and Irish coastline. Studies on sediment cores from the NE Atlantic margin showed a similar enrichment in IRD during the YD that was attributed largely to the Laurentide Ice Sheet, with the potential contribution of a calving ice sheet in Scotland (Scourse et al. 2009). Given the common petrologies (Bailey et al. 2013), another potential source for the YD IRD is the Scandinavian Ice Sheet (SIS), which is documented to have had a period of marine expansion south-west of Norway at the time (Broecker et al. 2010; Mangerud et al. 2016) and may have contributed icebergs flowing to the south. Further evidence based on microfossils suggests that the main oceanic currents flowing towards the north weakened, similarly to what happened during the previous glacial period, thus allowing the southward flow of icebergs with surface currents (Austin & Kroon 2001; Peck et al. 2006; Adams et al. 1999; Broecker et al. 2010; Lynch-Stieglitz et al. 2011). At this stage, it is not possible to distinguish which of these sources have or have not contributed to the distinct IRD peak at the YD on the DBF and further geochemical and petrological analyses are needed to assess iceberg provenance in this region.

### ***Comparison with other glaciated margins***

Most of the JC106 sediment record from the DBF is interpreted as representing the sedimentation occurring during the final stages of the last BIIS deglaciation, at the end of the last glacial (MIS2). Between ~18 and ~16 ka cal. BP, the DBF received meltwater and IRD from the BIIS before complete ice-depletion. This suggests that meltwater and iceberg discharge during the latter part of the deglaciation significantly contribute to the build-up of the DBF, in addition to the downslope sediment transport observed occurring during the broader last glacial interval (Howe 1995; Stoker 1995; Armishaw et al. 1998; Holmes et al. 1998; Sejrup et al. 2005).

The DBF deglaciation sediment record analysed in this study shows similarities with most records of other glaciated margins and glaciogenic fans. These similarities are recognised in the style of sediment deposition, in particular the presence of plumites, recognised along the Northern North Sea, the Norwegian Margin, the Barents Sea and the Canadian Slope (Hesse et al. 1999; Lekens et

al. 2006; Lucchi et al. 2015). The sedimentation rates calculated for the plumites on the Norwegian margin vary between 20 and 2000 cm/ka (Lekens et al. 2005; Hjelstuen et al. 2009). In addition, along the southern Norwegian margin, high content of IRD within plumites is correlated to the cessation of ice stream activity through calving events (Lekens et al. 2005).

Our data show that the deep water environments are still largely influenced by BIIS-related processes until the final stages of marine ice sheet extension. While when the ice sheet was positioned at the shelf break during glacial maxima, glaciogenic sediment deposition on the fan was dominated by downslope mass transport (Howe 1995; Armishaw et al. 1998; Holmes et al. 1998), the delivery of glacially-derived sediment to the fan during deglaciation, once the ice sheet retreated from the shelf edge, occurred largely by meltwater processes and iceberg rafting as testified by the presence of plumites and distinct IRD peaks within them. The meters-thick plumite intervals on the DBF also demonstrate that marine-terminating ice sheets are still able to deliver sediments with relatively high sedimentation rates through meltwater plumes at over 100 km distance from the ice margin.

More widely this highlights differences in the nature of sediment delivery on glaciated continental margins. High-latitude slopes, along the Norwegian and Svalbard margins (e.g., Dahlgren & Vorren 2003; Jessen et al. 2010), are dominated by downslope sediment transport, especially related to glaciogenic debris flows (Laberg et al. 2000); whereas, further south along the Irish margin and on the DBF the contribution of meltwater delivery becomes much more significant (Sacchetti et al. 2012a; this study). This is also consistent with studies from the Canadian margin, in particular the Scotian slope (e.g., Piper 1988), where meltwater delivery was a major contributor to margin development during the deglaciation phases of the Laurentide Ice Sheet (LIS). The ice loss from the southern portion of the LIS is inferred to have occurred mostly by melting due to the thermal gradient along the margin (Piper 1988); a similar thermal gradient could be the cause of the varying style of ice loss along the NE Atlantic discussed here.

#### ***Implication for climate reconstruction in the North Atlantic***

BIIS calving events have previously been interpreted as independently regulated by the internal ice-sheet dynamics on a millennial (D-O) time scale (Knutz et al. 2001; Wilson et al. 2002; Peck et al. 2006; Haapaniemi et al. 2010). From a broad perspective, a synchronicity in the final deglaciation of European Ice Sheets (EIS), including the BIIS, the Scandinavian Ice Sheet, the Svalbard-Barents-Kara Seas and the Channel River Hydrographic Network, along the North East Atlantic has been suggested (Hughes et al. 2015). The EIS, which similarly to the Laurentide Ice Sheet (LIS) delivered large amounts of freshwater to the North Atlantic Ocean, are also considered responsible for global climatic changes during the deglaciation (Bigg et al. 2012; Toucanne et al. 2015).

The BIIS dynamics, together with the other components of EIS, can therefore be considered as having an active and contributing role on the North Atlantic climate. The reconstructed dynamic behaviour of the BIIS from the DBF sediment record seems to show some synchronicity with the ice margin further south. In particular, sediment retrieved from the Bay of Biscay showed two large discharges of meltwater from the EIS occurring at  $18.2 \pm 0.2$  and  $16.7 \pm 0.2$  ka cal. BP (Toucanne et al. 2015). These timings are very similar to those of the DBF IRD peaks and inferred as large meltwater pulses and calving events during the deglaciation of the MSs and the HIS. Additionally, both the DBF and Bay of Biscay records show glacial instability and ice wasting during Heinrich stadial 1 (HS1) (18.2-16.7 ka BP), which represents the time period when instability of the LIS reached its maximum, including the occurrence of the Heinrich 1 event (Heinrich 1988). The synchronicity in the deglacial meltwater release between the BIIS and the EIS, and further afield with the LIS, highlights a potential climatic relationship among the circum-North Atlantic ice-sheets, at least in their final deglaciation. Given the potential effect of the release of large amount of meltwater on the North Atlantic circulation, it is possible that these pulses in deglaciation may explain some of the observed variability in the North Atlantic Ocean circulation at this time (cf. Bigg et al. 2012).

## Conclusions

The investigation of the deep water sediments retrieved from the DBF allowed for the reconstruction of the final stages of the BIIS deglaciation on the Malin Sea shelf, since 18 ka cal. BP, and the transition to modern climatic conditions (Fig. 8).

- The DBF sediments record deposition from meltwater plumes with high sedimentation rates during the final BIIS deglaciation, with a post-glacial restoration of ocean currents and deposition of contourites during the Holocene.
- Two intervals of iceberg calving during deglaciation are identified, at ~17.8 and ~16.9 ka cal. BP. These occurred within the period when meltwater released by the demise of the MSs sector of the BIIS resulted in the deposition of thick plumites on the DBF.
- The BIIS meltwater pulses and calving events recorded by the DBF cores appear to be largely synchronous with those from other European Ice Sheets at the transition between MIS 2 and MIS 1. This possible Pan-European synchronous behavior with the release of large amounts of freshwater could have had an active role on the reduction of the Atlantic Meridional Oceanic Current at this time and ensuing effects on the North Atlantic climate.
- The DBF sediment record also include an IRD-rich interval during the Younger Dryas. Whilst it is not possible to discern the source of icebergs in this region at the time, the distinct IRD peak coupled with previously published geomorphological evidence of iceberg scouring at the shelf edge suggests a significant presence of icebergs at this latitude in the NE Atlantic during the YD.
- The transition into post-glacial conditions is marked by the ichnofacies *Zoophycos* indicating interstadial climatic conditions and the restoration of oceanic currents. Post-glacial sedimentation is characterised by contouritic deposition. The condensed sediment record at the core tops suggest much lower sedimentation rates in the Holocene than during deglaciation and sediment starvation of the margin.

## Acknowledgments

ST acknowledges Ulster University's Vice-Chancellor Research Scholarship for support to her PhD 2014-2017. This research was funded by the UK Natural Environment Research Council grant NE/J007196/1 'BRITICE-CHRONO'. We thank the officers and crew of the *RRS James Cook* for their help with data acquisition. We also thank Stephen Livingstone, Kasper Weilbach, Riccardo Arosio, Catriona Purcell, Zoe Roseby and Elke Hanenkamp for their scientific support on the JC106 Leg 2 cruise. The authors wish to acknowledge support from the School of Radiology at Ulster University for the X-radiographs acquisition, the UK Natural Environment Research Council (NERC) Radiocarbon Facility (NRCF-East Kilbride) and the commercial analytical laboratory Beta Analytic for the radiocarbon dating. Thanks to Ruth Plets and William Austin for the discussion during the PhD viva and all comments they provided to an earlier version of the manuscript included in ST's thesis. Also thanks to the SGJ reviewers and editors for their comments, which helped in improving the manuscript and allowed us the time to do so. The work was supported by the NERC Radiocarbon Facility Allocation No. 1722.0613 and 1878.1014.



## References

- Adams, J., Maslin, M., Thomas, E., 1999. Sudden climate transitions during the Quaternary. *Progress in Physical Geography*, 23(1), 1-36.
- Aksu, A.E., Hiscott, R.N., 1989. Slides and debris flows on the high-latitude continental slope of Baffin Bay. *Geology*, 17(10), 885-888.
- Alley, R.B., 2000. The Younger Dryas cold interval as viewed from central Greenland. *Quaternary Science Reviews*, 19(1–5), 213-226.
- Andrews, J.T., 2000. Icebergs and iceberg rafted detritus (IRD) in the North Atlantic: facts and assumptions. *Oceanography*, 13,3/2000, 100-108.
- Armishaw, J.E., Holmes, R.W., Stow, D.A.V., 1998. Morphology and sedimentation on the Hebrides Slope and Barra Fan, NW UK continental margin. *Geological Processes on Continental Margins: Sedimentation, Mass-Wasting and Stability*. Geological Society, London, Special Publications, 129, 81-104.
- Arosio R., Crocket K.C., Nowell G.M., Callard S.L., Howe J.A., Benetti S., Fabel D., Moreton S., Clark C.D. (2018) Weathering fluxes and sediment provenance on the SW Scottish shelf during the last deglaciation. *Marine Geology*, 42: 81-98
- Austin, W. E. N., Kroon, D., 2001. Deep sea ventilation of the northeastern Atlantic during the last 15,000 years. *Global and Planetary Change*, 30(1-2), 13-31.
- Bailey, I., Hole, G.M., Foster, G.L., Wilson, P.A., Storey, C.D., Trueman, C.N., Raymo, M.E. 2013. An alternative suggestion for the Pliocene onset of major northern hemisphere glaciation based on the geochemical provenance of North Atlantic Ocean ice-rafted debris. *Quaternary Science Reviews*, 75, 181-194.

- Ballantyne, C.K., Ó Cofaigh, C., 2017. The last Irish Ice Sheet: extent and chronology. *Advances in Irish Quaternary Studies*, 1, 101-149.
- Ballantyne, C.K., Stone, J.O., McCarroll, D., 2008. Dimensions and chronology of the last ice sheet in western Ireland. *Quaternary Science Reviews* 27: 185–200.
- Benetti, S., 2006. Late Quaternary sedimentary processes along the western North Atlantic margin. Ph.D. thesis, Graduate School of the National Oceanography Centre, Southampton, U.K., 204 p.
- Benetti, S., Dunlop, P., Ó Cofaigh, C., 2010. Glacial and glacially-related geomorphology of the north-west Irish continental margin. *Journal of Maps*, 30-39.
- Bigg, G.R., Clark, C.D., Greenwood, S.L., Haflidason, H., Hughes, A.L.C., Levine, R.C., Nygård, A., Sejrup, H.P., 2012. Sensitivity of the North Atlantic circulation to break-up of the marine sectors of the NW European ice sheets during the last Glacial: A synthesis of modelling and palaeoceanography. *Global and Planetary Change*, 98–99, 153-165.
- Bond, G.C., Broecker, W., Johnsen, S., McManus, J., Labeyrie, L., Jouzel, J., Bonani, G., 1993. Correlations between climate records from North Atlantic sediments and Greenland ice. *Letters to Nature*, 365, 143-147.
- Broecker, W.S., Denton, G.H., Edwards, R.L. and Cheng, H., Alley, R.B., Putnam, A.E., 2010. Putting the Younger Dryas cold event into context. *Quaternary Science Reviews*, 29(9–10), 1078-1081.
- Buckley, D.E., MacKinnon, W.G., Cranston, R.E. and Christian, H.A., 1994. Problems with piston core sampling: Mechanical and geochemical diagnosis. *Marine Geology*, 117(1-4), 95-106.
- Callard, S.L., Ó Cofaigh, C., Benetti, S., Chiverrell, R.C., Van Landeghem, K. J.J., Saher, M.H., Gales J.A., Small, D., Clark, C.D., Livingstone, S.J., Fabel, D., Moreton, S.G., 2018. Extent and

retreat history of the Barra Fan Ice Stream offshore western Scotland and northern Ireland during the last glaciation. *Quaternary Science Reviews*, 201, 280-302.

Chiverrell, R.C., Thomas, G.S.P., 2010. Extent and timing of the Last Glacial Maximum (LGM) in Britain and Ireland: a review. *Journal of Quaternary Science*, 25(4), 535-549.

Clark, C.D., Hughes, A.L.C., Greenwood, S.L., Jordan, C., Sejrup, HP., 2012. Pattern and timing of retreat of the last British-Irish Ice Sheet. *Quaternary Science Reviews*, 44, 112-146.

Dahlgren, K.T., Vorren, T.O., 2003. Sedimentary environment and glacial history during the last 40 ka of the Vøring continental margin, mid-Norway. *Marine Geology*, 193(1-2), 93-127.

Dickson, R.R., Kidd, R.B., 1987. Deep circulation in the southern Rockall Trough-the oceanographic setting of site-610. *Initial Reports of the Deep Sea Drilling Project*, 94, 1061-1074.

Dorador, J., Wetzel, A., Rodríguez-Tovar, F.J., 2016. *Zoophycos* in deep-sea sediments indicates high and seasonal primary productivity: Ichnology as a proxy in palaeoceanography during glacial–interglacial variations. *Terra Nova*, 28(5), 323-328.

Dove, D., Arosio, R., Finlayson, A., Bradwell, T., Howe, J.A., 2015. Submarine glacial landforms record Late Pleistocene ice-sheet dynamics, Inner Hebrides, Scotland. *Quaternary Science Reviews*, 123, 76-90.

Dowdeswell, J.A., Elverhfi, A., Spielhagen, R., 1998. Glacimarine sedimentary processes and facies on the polar north Atlantic margins. *Quaternary Science Reviews*, 17(1), 243-272.

Dunlop, P., Shannon, R., McCabe, M., Quinn, R., Doyle, E., 2010. Marine geophysical evidence for ice sheet extension and recession on the Malin Shelf: New evidence for the western limits of the British Irish Ice Sheet. *Marine Geology*, 276, 86-99.

Faugeres, J.C, Gonthier, E., Grousset, F., Poutiers, J., 1981. The Feni Drift: The importance and meaning of slump deposits on the eastern slope of the Rockall Bank. *Marine Geology*, 40(3), M49-M57.

Finlayson, A., Fabel, D., Bradwell, T. and Sugden, D., 2014. Growth and decay of a marine terminating sector of the last British–Irish Ice Sheet: a geomorphological reconstruction. *Quaternary Science Reviews*, 83, 28-45.

García, M., Ercilla, G., Alonso, B., Casas, D., Dowdeswell, J.A., 2011. Sediment lithofacies, processes and sedimentary models in the Central Bransfield Basin, Antarctic Peninsula, since the Last Glacial Maximum. *Marine Geology*, 290(1), 1-16.

Georgiopoulou, A., Benetti, S., Shannon, P., Haughton, P.D.W., McCarron, S., 2012. Gravity flow deposits in the deep Rockall Trough, northeast Atlantic. In: Yamada, Y.e.a. ed. *Submarine mass movements and their consequences, Advances in natural and technological hazards research*. 31st ed. Netherlands: Springer, 695-707.

Haapaniemi, A.I., Scourse, J.D., Peck, V.L., Kennedy, H., Kennedy, P., Hemming, S.R., Furze, M.F.A., Pienkowski, A.J., Austin, W.E.N., Walden, J., Wadsworth, E., Hall, I.R., 2010. Source, timing, frequency and flux of ice-rafted detritus to the Northeast Atlantic margin, 30-12 ka: testing the Heinrich precursor hypothesis. *Boreas an International Journal of Quaternary Research*, 39, 576-591.

Heinrich, H., 1988. Origin and consequences of cyclic ice rafting in the Northeast Atlantic Ocean during the past 130,000 years. *Quaternary Research*, 29(2), 142-152.

Hesse, R., Khodabakhsh, S., Klaucke, I., Ryan, W.B.F., 1997. Asymmetrical turbid surface-plume deposit near ice-outlets of the Pleistocene Laurentide ice sheet in the Labrador Sea. *Geo-Marine Letters*, 17(3), 179-187.

Hesse, R., Klauck, I., Khodabakhsh, S., Piper, D., 1999. Continental slope sedimentation adjacent to an ice margin. III. The upper Labrador Slope. *Marine Geology*, 155(3–4), 249-276.

Hjelstuen, B.O., Haflidason, H., Sejrup, H.P., Lyså, A., 2009. Sedimentary processes and depositional environments in glaciated fjord systems - Evidence from Nordfjord, Norway. *Marine Geology*, 258(1-4), 88-99.

Hibbert, F.D., Austin, W.E.N., Leng, M.J., Gatliff, R.W. (2010) British Ice Sheet dynamics inferred from North Atlantic ice-rafted debris records spanning the last 175 000 years. *Journal of Quaternary Science*, 25(4), 461-482.

Holliday, P.N., Pollard, R.T., Read, J.F., Leach, H., 2000. Water mass properties and fluxes in the Rockall Trough, 1975–1998. *Deep Sea Research Part I: Oceanographic Research Papers*, 47(7), 1303-1332.

Holmes, R., Long, D., Dodd, L.R., 1998. Large-scale debrites and submarine landslide on the Barra Fan, west of Britain. *Geological Processes on Continental Margins: Sedimentation, Mass-Wasting and Stability*. Geological Society, London, Special Publications, 129, 67-79.

Howe, J.A., 1995. Sedimentary processes and variations in slope-current activity during the last Glacial-Interglacial episode on the Hebrides Slope, northern Rockall Trough, North Atlantic Ocean. *Sedimentary Geology*, 96(3), 201-230.

Howe, J.A., 1996. Turbidite and contourite sediment waves in the northern Rockall Trough, North Atlantic Ocean. *Sedimentology*, 43, 219-234.

Howe, J.A., Harland, R., Hine, N.M., Austin, W.E.N., 1998. Late Quaternary stratigraphy and palaeoceanographic change in the northern Rockall Trough, North Atlantic Ocean. *Geological Processes on Continental Margins: Sedimentation, Mass-Wasting and Stability*. Geological Society, London, Special Publications, 129, 269-286.

Howe, J.A., Dove, D., Bradwell, T., Gafeira, J., 2012. Submarine geomorphology and glacial history of the Sea of the Hebrides, UK. *Marine Geology*, 315-318(Supplement C), 64-76.

Hughes, A.L.C., Gyllencreutz, R., Lohne O.S., Mangerud, J., Svendsen J.I., 2015. The last Eurasian Ice Sheet - a chronological database and time-slice reconstruction, DATED-1. *Boreas an International Journal of Quaternary Research*, 45, 1-45.

Jessen, S.P., Rasmussen, T.L., Nielsen, T., Solheim, A., 2010. A new Late Weichselian and Holocene marine chronology for the western Svalbard slope 30,000–0 cal years BP. *Quaternary Science Reviews*, 29(9-10), 1301-1312.

Knutz, P.C., Austin, W.E.N., Jones, E.J.W., 2001. Millennial-scale depositional cycles related to British Ice Sheet variability and North Atlantic palaeocirculation since 45 kyrs B.P., Barra fan, U.K. margin. *Paleoceanography*, 16, 53-64.

Knutz, P.C., Jones, E.J.W., Austin, W.E.N., van Weering, T.C.E., 2002. Glacimarine slope sedimentation, contourite drifts and bottom current pathways on the Barra Fan, UK North Atlantic margin. *Marine Geology*, 188(1–2), 129-146.

Lekens, W.A.H., Sejrup, H.P., Haflidason, H., Petersen, G.Ø., Hjelstuen, B., Knorr, G., 2005. Laminated sediments preceding Heinrich event 1 in the Northern North Sea and Southern Norwegian Sea: origin, processes and regional linkage. *Marine Geology*, 216(1-2), 27-50.

Lisiecki, L. E., Raymo, M.E., 2005. A Pliocene-Pleistocene stack of 57 globally distributed benthic  $\delta^{18}\text{O}$  records. *Paleoceanography*, 20(1), PA1003.

Lowe, D.R., 1979. Sediment gravity flows: their classification and some problems of application to natural flows and deposits. In: Doyle, L.J., Pilkey, O.H. ed. *Geology of continental slopes*. Special Publication, 27 ed. Tulsa, Oklahoma: Society of economic paleontologists and mineralogists, 75-84.

- Lowe, D.R., 1982. Sediment gravity flows: II. Depositional models with special reference to the deposits of high density turbidity currents. *Journal of Sedimentary Petrology*, 52, 279-297.
- Löwemark, L., Lin, H.L., Sarnthein, M., 2006. Temporal variations of the trace fossil *Zoophycos* in a 425 ka long sediment record from the South China Sea: implications for the ethology of the *Zoophycos* producer. *Geological Magazine*, 143(1), 105-114.
- Lucchi, R.G., Rebesco, M., Camerlenghi, A., Busetti, M., Tomadin, L., Villa, G., Persico, D., Morigi, C., Bonci, M.C., Giorgetti, G., 2002. Mid-late Pleistocene glacimarine sedimentary processes of a high-latitude, deep-sea sediment drift (Antarctic Peninsula Pacific margin). *Marine Geology*, 189(3–4), 343-370.
- Lucchi, R.G., Sagnotti, L., Camerlenghi, A., Macrì, P., Rebesco, M., Pedrosa, M.T., Giorgetti, G., 2015. Marine sedimentary record of Meltwater Pulse 1a along the NW Barents Sea continental margin. *arktos*, 1(1), 7.
- Lynch-Stieglitz, J., Schmidt, M.W., Curry, W.B., 2011. Evidence from the Florida Straits for Younger Dryas ocean circulation changes. *Paleoceanography*, 26(1), PA1205.
- Mangerud, J., Aarseth, I., Hughes, A.L.C., Lohne, Ø.S., Skår, K., Sønstegaard, E., Svendsen, J.I., 2016. A major re-growth of the Scandinavian Ice Sheet in western Norway during Allerød-Younger Dryas. *Quaternary Science Reviews*, 132, 175-205.
- Masson, D.G., Plets, R.M.K., Huvenne, V.A.I., Wynn, R.B., Bett, B.J., 2010. Sedimentology and depositional history of Holocene sandy contourites on the lower slope of the Faroe–Shetland Channel, northwest of the UK. *Marine Geology*, 268(1), 85-96.
- McCartney, M.S., 1992. Recirculating components to the deep boundary current of the northern North Atlantic. *Progress in Oceanography*, 29(4), 283-383.

McManus, J.F., Francois, R., Gherardi, J.M., Keigwin, L.D., Brown-Leger, S., 2004. Collapse and rapid resumption of Atlantic meridional circulation linked to deglacial climate change. *Letter to Nature*, 428, 834-837.

Middleton, G.V., Hampton, M.A., 1976. Subaqueous sediment transport and deposition by sediment gravity flows. *Marine Sediment Transport* (Eds.D.J.Stanley and D.J.P.Swift), 197-218. Wiley, New York.

Mingard, K., Morrell, R., Jackson, P., Lawson, S., Patel, S., Buxton, R., 2009. Good practice guide for improving the consistency of particle size measurements. NPL Report, ISSN 1368-6550, Teddington, Middlesex.

Mitchum, R.M., Vail, P.R., Sangree, J.B., 1977. Seismic stratigraphy and global changes of sea level: Part 6. Stratigraphic interpretation of seismic reflection patterns in depositional sequences: Section 2. Application of seismic reflection configuration to stratigraphic interpretation. In: Anon. *Seismic stratigraphy- applications to hydrocarbon exploration*. AAPG Special Volumes, 117-133.

New, A.L., Smythe-Wright, D., 2001. Aspects of the circulation in the Rockall Trough. *Continental Shelf Research*, 21(8–10), 777-810.

Ó Cofaigh, C., Dowdeswell, J.A., 2001. Laminated sediments in glacialmarine environments: diagnostic criteria for their interpretation. *Quaternary Science Reviews*, 20(13), 1411-1436.

Ó Cofaigh, C., Dunlop, P., Benetti, S., 2012. Marine geophysical evidence for Late Pleistocene ice sheet extent and recession off northwest Ireland. *Quaternary Science Reviews*, 44, 147-159.

Owen, M.J., Maslin, M.A., Day, S.J. and Long, D., 2018. Sediment failures within the Peach Slide (Barra Fan, NE Atlantic Ocean) and relation to the history of the British-Irish Ice Sheet. *Quaternary Science Reviews*, 187, 1-30.



- Peck, V.L., Hall, I.R., Zahn, R., Elderfield, H., Grousset, F., Hemming, S.R., Scourse, J.D., 2006. High resolution evidence for linkages between NW European ice sheet instability and Atlantic Meridional Overturning Circulation. *Earth and Planetary Science Letters*, 243(3–4), 476–488.
- Peck, V.L., Hall, I.R., Zahn, R., Grousset, F., Hemming, S.R., Scourse, J.D., 2007. The relationship of Heinrich events and their European precursors over the past 60 ka BP: a multi-proxy ice-rafted debris provenance study in the North East Atlantic. *Quaternary Science Reviews*, 26(7–8), 862–875.
- Peters, J.L., Benetti, S., Dunlop, P., Ó Cofaigh, C., 2015. Maximum extent and dynamic behaviour of the last British–Irish Ice Sheet west of Ireland. *Quaternary Science Reviews*, 128, 48–68.
- Piper, D.J. (1988) DNAG# 3. Glaciomarine sedimentation on the continental slope off eastern Canada. *Geoscience Canada*, 15(1).
- Piper, D.J.W., 2005. Late Cenozoic evolution of the continental margin of eastern Canada. *Norwegian Journal of Geology*, 85, 305–318.
- Piper, D.J. and Normark, W.R., 2009. Processes that initiate turbidity currents and their influence on turbidites: a marine geology perspective. *Journal of Sedimentary Research*, 79(6), 347–362.
- Prothro, L.O., Simkins, L.M., Majewski, W., Anderson, J.B., 2018. Glacial retreat patterns and processes determined from integrated sedimentology and geomorphology records. *Marine Geology*, 395, 104–119.
- Rahmstorf, S., 2002. Ocean circulation and climate during the past 120,000 years. *Nature*, 419(6903), 207–214.
- Ramsey, C.B., 2009. Bayesian analysis of radiocarbon dates. *Radiocarbon*, 51(1), 337–360.

Rashid, H., Piper, D.J.W., MacKillop, K., Ouellette, D., Vermooten, M., Muñoz, A., Jiménez, P., 2019. Dynamics of sediments on a glacially influenced, sediment starved, current-swept continental margin: The SE Grand Banks Slope off Newfoundland. *Marine Geology*, 408, 67-86.

Rasmussen, S.O., Bigler, M., Blockley, S.P., Blunier, T., Buchardt, S.L., Clausen, H.B., Cvijanovic, I., Dahl-Jensen, D., Johnsen, S.J., Fischer, H., Gkinis, V., Guillevic, M., Hoek, W.Z., Lowe, J.J., Pedro, J.B., Popp, T., Seierstad, I.K., Steffensen, J.P., Svensson, A.M., Vallelonga, P., Vinther, B.M., Walker, M.J.C., Wheatley, J.J., Winstrup, M., 2014. A stratigraphic framework for abrupt climatic changes during the Last Glacial period based on three synchronized Greenland ice-core records: refining and extending the INTIMATE event stratigraphy. *Quaternary Science Reviews*, 106(Supplement C), 14-28.

Read, J.F., 2000. CONVEX-91: water masses and circulation of the Northeast Atlantic subpolar gyre. *Progress in Oceanography*, 48(4), 461-510.

Rebesco, M., Hernández-Molina, F.J., Van Rooij, D., Wåhlin, A., 2014. Contourites and associated sediments controlled by deep-water circulation processes: State-of-the-art and future considerations. *Marine Geology*, 352, 111-154.

Reimer, P.J., Bard, E., Bayliss, A., Beck, J.W., Blackwell, P.G., Ramsey, C.B., Buck, C.E., Cheng, H., Edwards, R.L., Friedrich, M., Grootes, P.M., Guilderson, T.P., Haflidason, H., Hajdas, I., Hatté, C., Heaton, T.J., Hoffmann, D.L., Hogg, A.G., Hughen, K.A., Kaiser, K.F., Kromer, B., Manning, S.W., Niu, M., Reimer, R.W., Richards, D.A., Scott, E.M., Southon, J.R., Staff, R.A., Turney, C.S.M., van der Plicht, J., 2013. IntCal13 and Marine13 Radiocarbon Age Calibration Curves 0–50,000 Years cal BP. *Radiocarbon*, 55(4), 1869-1887.

Roger, J., Saint-Ange, F., Lajeunesse, P., Duchesne, M.J., St-Onge, G., 2013. Late Quaternary glacial history and meltwater discharge along the northeastern Newfoundland shelf. *Canadian Journal of Earth Sciences*, 50, 1178-1194.

- Rørvik, K.L., Laberg, J.S., Hald, M., Ravna, E.K., Vorren, T.O., 2010. Behavior of the northwestern part of the Fennoscandian Ice Sheet during the Last Glacial Maximum—a response to external forcing. *Quaternary Science Reviews*, 29(17-18), 2224-2237.
- Sacchetti, F., Benetti, S., Georgiopoulou, A., Shannon, P.M., O'Reilly, B.M., Dunlop, P., Quinn, R., Ó Cofaigh, C., 2012a. Deep-water geomorphology of the glaciated Irish margin from high-resolution marine geophysical data. *Marine Geology*, 291–294, 113-131.
- Sacchetti, F., Benetti, S., Ó Cofaigh, C., Georgiopoulou, A., 2012b. Geophysical evidence of deep-keeled icebergs on the Rockall Bank, Northeast Atlantic Ocean. *Geomorphology*, 159–160, 63-72.
- Scourse, J.D., Haapaniemi, A.I., Colmenero-Hidalgo, E., Peck, V.L., Hall, I.R., Austin, W.E.N., Knutz, P.C., Zahn, R., 2009. Growth, dynamics and deglaciation of the last British–Irish ice sheet: the deep-sea ice-rafted detritus record. *Quaternary Science Reviews*, 28(27–28), 3066-3084.
- Sejrup, H-P., Hjelstuen, B.O., Torbjørn, D.K.I., Haflidason, H., Kuijpers, A., Nygård, A., Praeg, S., Stoker, M.S., Vorren, T.O., 2005. Pleistocene glacial history of the NW European continental margin. *Marine and Petroleum Geology*, 22(9–10), 1111-1129.
- Small, D., Rinterknecht, V., Austin, W.E., Bates, R., Benn, D.I., Scourse, J.D., Bourlès, D.L., Hibbert, F.D. and ASTER Team, 2016. Implications of  $^{36}\text{Cl}$  exposure ages from Skye, northwest Scotland for the timing of ice stream deglaciation and deglacial ice dynamics. *Quaternary Science Reviews*, 150, 130-145.
- Small, D., Benetti, S., Dove, D., Ballantyne, C.K., Fabel, D., Clark, C.D., Gheorghiu, D.M., Newall, J., Xu, S., 2017. Cosmogenic exposure age constraints on deglaciation and flow behaviour of a marine-based ice stream in western Scotland, 21–16 ka. *Quaternary Science Reviews*, 167, 30-46.

Stanford, J.D., Rohling, E.J., Bacon, S., Roberts, A.P., Grousset, F.E., Bolshaw, M., 2011. A new concept for the paleoceanographic evolution of Heinrich event 1 in the North Atlantic. *Quaternary Science Reviews*, 30(9–10), 1047-1066.

Stoker, M.S., 1995. The influence of glacigenic sedimentation on slope-apron development on the continental margin off Northwest Britain. *The Tectonics, Sedimentation and Palaeoceanography of the North Atlantic Region*, Geological Society Special Publication, 90, 159-177.

Stoker, M.S., 1997. Mid- to late Cenozoic sedimentation on the continental margin off NW Britain. *Journal of the Geological Society*, London, 154, 509-515.

Stoker, M.S., Leslie, A.B., Scott, W.D., Briden, J.C., Hine, N.M., Harland, R., Wilkinson, I.P., Evans, D., Ardur, D.A., 1994. A record of late Cenozoic stratigraphy, sedimentation and climate change from the Hebrides Slope, NE Atlantic Ocean. *Journal of the Geological Society*, 151(2), 235-249.

Stoker, M.S., Praeg, D., Hjelstuen, B.O., Laberg, J.S., Nielsen, T., Shannon, P.M., 2005. Neogene stratigraphy and the sedimentary and oceanographic development of the NW European Atlantic margin. *Marine and Petroleum Geology*, 22(9–10), 977-1005.

Stow, D.A.V., 1979. Distinguishing between fine-grained turbidites and contourites on the Nova Scotia deep water margin. *Sedimentology*, 26, 371-387.

Stow, D.A.V., Lovell, J.P.B., 1979. Contourites: Their recognition in modern and ancient sediments. *Earth-Science Reviews*, 14(3), 251-291.

Stow, D.A.V., Piper, D.J.W., 1984. Deep-water fine-grained sediments: facies models. *Fine-Grained Sediments: Deep Water Processes and Facies*. Blackwell Scientific Publication for the Geological Society, 661-644.

Stow, D.A.V., Reading, H.G., Collinson, J.D., 1996. Deep seas. *Sedimentary Environments: Processes, Facies and Stratigraphy*, 3, 395-453.

Stow, D.A.V., Mayall, M., 2000. Deep-water sedimentary systems: New models for the 21st century. *Marine and Petroleum Geology*, 17(2), 125-135.

Stow, D.A.V., Faugeres, J-C., Howe, J.A., Pudsey, C.J., Viana, A.R., 2002. Bottom currents, contourites and deep-sea sediment drift: current state-of-the-art. *Deep-Water Contourite Systems: Modern Drifts and Ancient Series, Seismic and Sedimentary Characteristics*. Geological Society, London, Memoirs, 22, 7-20.

Tarlati, S. 2018. Late Quaternary reconstruction of British-Irish Ice Sheet variability through the analysis of deep-water sediments from the Donegal Barra Fan and the Rockall Trough, North Atlantic. Unpublished PhD Thesis, Ulster University, 204 pp.

Toucanne, S., Soulet, G., Freslon, N., Silva Jacinto, R., Dennielou, B., Zaragosi, S., Eynaud, F., Bourillet, J.F., Bayon, G., 2015. Millennial-scale fluctuations of the European Ice Sheet at the end of the last glacial, and their potential impact on global climate. *Quaternary Science Reviews*, 123, 113-133.

Tripsanas, E.K., Piper, D.J.W., 2008. Glaciogenic debris-flow deposits of Orphan Basin, offshore eastern Canada: sedimentological and rheological properties, origin, and relationship to meltwater discharge. *Journal of Sedimentary Research*, 78(11), 724-744.

Van Landeghem, K.J., Wheeler, A.J., Mitchell, N.C., 2009. Seafloor evidence for palaeo-ice streaming and calving of the grounded Irish Sea Ice Stream: Implications for the interpretation of its final deglaciation phase. *Boreas*, 38, 119-131.

Wanamaker Jr, A.D., Butler, P.G., Scourse, J.D., Heinemeier, J., Eiríksson, J., Knudsen, K.L., Richardson, C.A., 2012. Surface changes in the North Atlantic meridional overturning circulation during the last millennium. *Nature Communications*, 3, 899.

Wang, D., Hesse, R., 1996. Continental slope sedimentation adjacent to an ice-margin. II. Glaciomarine depositional facies on labrador slope and glacial cycles. *Marine Geology*, 135(1), 65-96.

Weaver, P.P.E., Wynn, R.B., Kenyon, N.H., Evans, J., 2000. Continental margin sedimentation, with special reference to the north-east Atlantic margin. *Sedimentology*, 47(s1), 239-256.

Wilson, L.J., Austin, W.E.N., Jansen, E., 2002. The last British Ice Sheet: growth, maximum extent and deglaciation. *Polar Research*, 21(2), 243-250.

Wynn, R.B., Stow, D.A.V., 2002. Classification and characterisation of deep-water sediment waves. *Marine Geology*, 192(1), 7-22.

Figure 1: North Atlantic glaciated margin with the highlighted approximate extent of the Donegal Barra Fan (dashed black line; simplified from Sacchetti et al. 2012a) and JC106 core locations (red points) on the North Atlantic glaciated margin. The main inferred directions of ice streaming during the last glacial period are indicated by the black arrows (Hebrides Ice Stream-HIS from Western Scotland; North Channel Ice Stream-NCIS from North Ireland; Clark et al. 2012). Inset shows the position of the main map along the Atlantic margin with the main deep water masses. A-A': Location of seismic line presented in this paper (Fig. 2). DBF=Donegal-Barra Fan (outline from Sacchetti et al., 2012), MSs= Malin Sea shelf, OH= Outer Hebrides, RT=Rockall Trough, Hs= Hebrides Slope; HS=Hebrides Seamount, ADS=Anton Dohrn Seamount, NADW=North Atlantic Deep Water, ENAW=Eastern North Atlantic Water. Bathy-topography from GEBCO, General Bathymetric Chart of the Ocean, for the bathymetry data,

Figure 2: Seismic profile along the slope with core location for 134PC and 133PC. Insets are indicated for the a) lower slope, b) middle slope, c) upper slope. The acoustic facies identified are indicated by coloured lines.

Figure 3: Five lithofacies illustrated with x-radiographs. Foraminiferal-bearing mud: FM (identified by the yellow lateral bar); Extensively bioturbated mud: BM (*Zoophycos* burrows shown by orange arrows; this image is presented with inverted grey-colour scale to better display the ichnofacies); Chaotic mud: CM (purple arrow indicates an inclined shear surface); Laminated sand to mud couplet: LSM (fining upward of the sediment visible in the x-rays); Laminated mud rich in IRD: ILM (larger lithic grains indicated by blue arrows and laminations are visible in the x-rays).

Figure 4: X-radiographs, lithofacies identification, log, magnetic susceptibility (MS), mean volume grain size ( $\mu\text{m}$ ) (D), IRD concentration [IRD], abundance of *Neogloboquadrina pachyderma sinistral* (%NPS calculated as percentage of the total planktonic foraminiferal assemblage) and conventional radiocarbon ages for core JC106-133PC. MS data from Figs. 4 to 6, present a wider spacing, approximately every meter, in correspondence of the end of the core sections. Lithofacies:

FM=Foraminiferal-bearing mud, BM=Extensively bioturbated mud, CM=Chaotic mud, LSM=Laminated sand to mud couplet, ILM=Laminated mud rich in IRD.

Figure 5: X-radiographs, lithofacies identification, log, magnetic susceptibility (MS), mean volume grain size (D), IRD concentration [IRD] and conventional radiocarbon age for core JC106-128PC.

Figure 6: X-radiographs, lithofacies identification, log, magnetic susceptibility (MS), mean volume grain size (D), IRD concentration [IRD] and conventional radiocarbon ages for core JC106-134PC.

Figure 7: Correlation between the three DBF sediment cores based on lithofacies, [IRD] concentration and calibrated radiocarbon dates. The yellow arrow at the 128PC core top highlights the thin FM facies.

Figure 8: Schematic depositional model for the DBF. The sedimentation is represented by meltwater pulses, iceberg discharges and downslope mass transport. Meltwater and iceberg presence are recorded in sediments older than 15.9 ka cal. BP and of Younger Dryas age. Contouritic deposition is recognized for sediment dated after 15.5 ka cal. BP. Currents abbreviations: ENAW= Eastern North Atlantic Water; DNBC= Deep Northern Boundary Current.

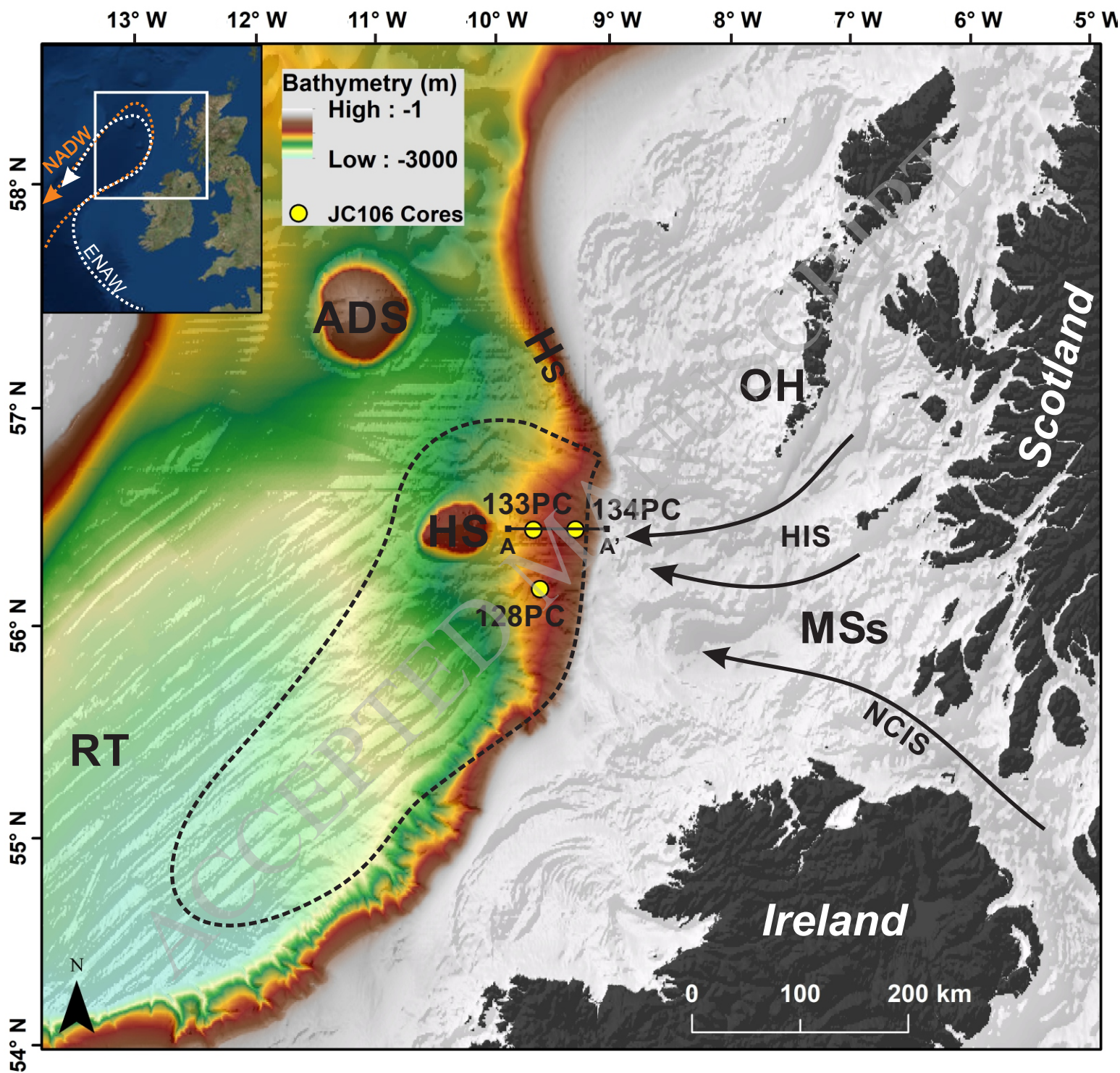


*Table 1: Sediment core information.*

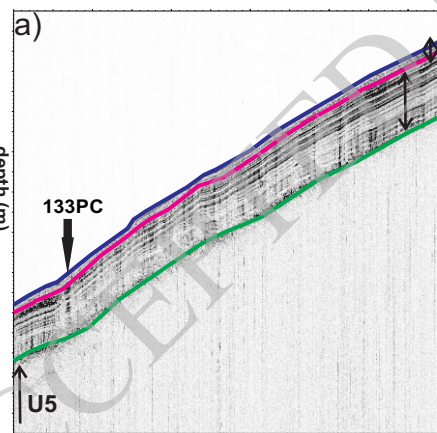
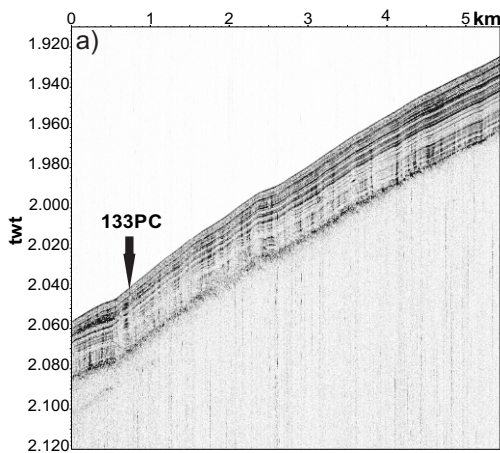
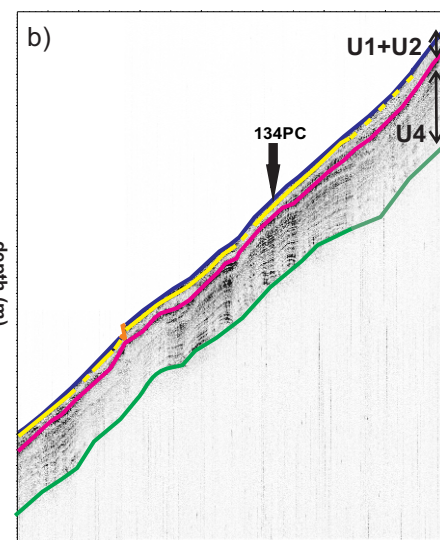
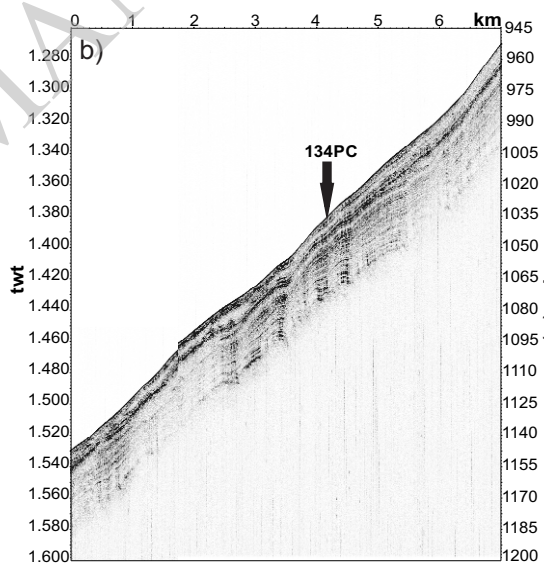
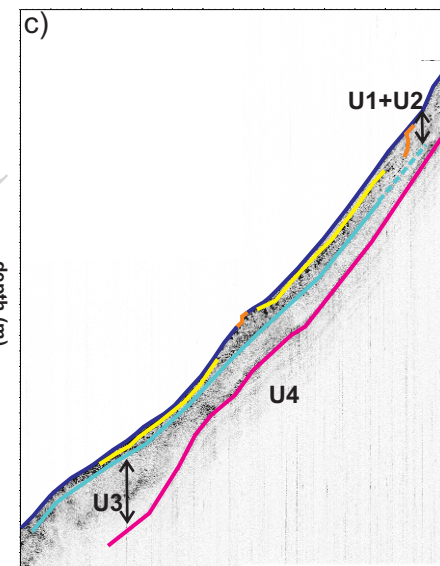
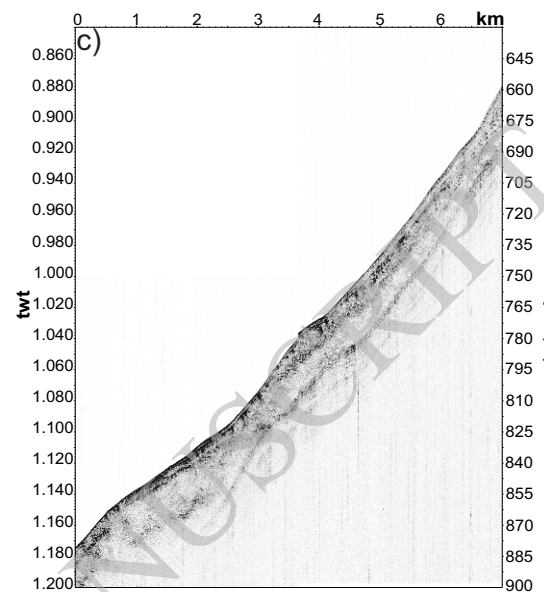
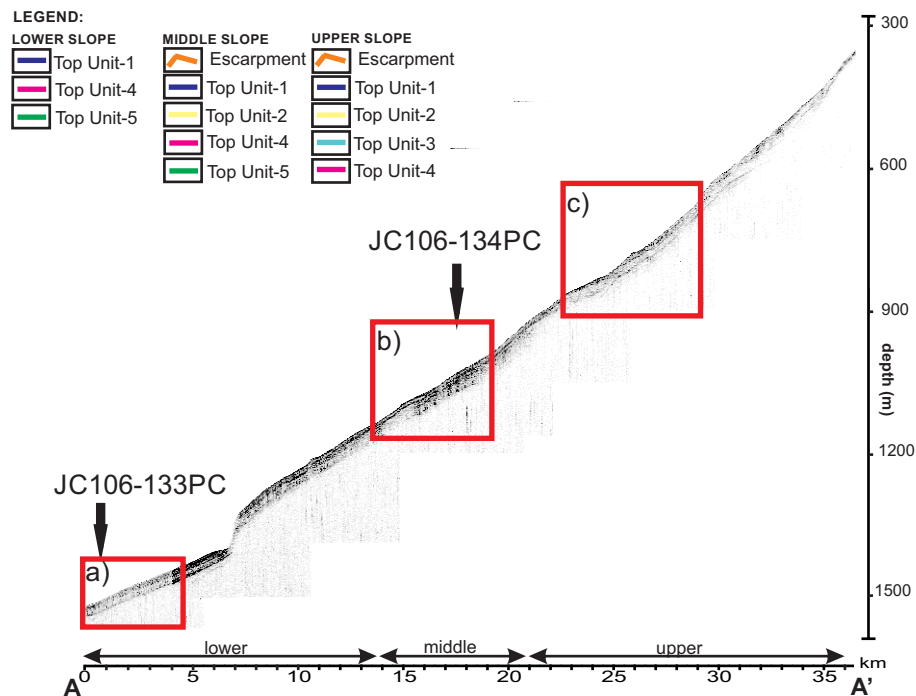
Core	Latitude (°N)	Longitude (°W)	Water depth (m)	Core Length (cm)
JC106-128PC	56.17147	9.616743	1475	668
JC106-133PC	56.44449	9.672212	1537	661
JC106-134PC	56.44471	9.321229	1036	672

Table 2: Radiocarbon results. Sample indicated by \* was not taken into account for age reconstruction as it was at a later stage recognized to be in a re-deposited/disturbed interval. All the values are rounded to the nearest decade or multiple of 5. NPS=Neogloboquadrina pachyderma sinistral, G.B.= Globigerina bulloides.

Core	Depth (cm)	Sample material	<sup>14</sup> C Age (yrs. BP)	Calibrated age (yrs. BP) $\Delta R=0$	Calibrated age (yrs. BP) $\Delta R=300$	Calibrated age (yrs. BP) $\Delta R=700$	Surrounding lithofacies	Laboratory code
128PC	125-128	Mono. NPS	13710 $\pm$ 40	15995 $\pm$ 180	15550 $\pm$ 220	14960 $\pm$ 230	LM	SUERC-67943
134PC	60-61	Mono. G.B.	13175 $\pm$ 40	15215 $\pm$ 140	14635 $\pm$ 360	13955 $\pm$ 135	EXFM	SUERC-63572
134PC	588-593	Mixed benthic forams	15020 $\pm$ 45	17800 $\pm$ 170	17445 $\pm$ 180	16865 $\pm$ 225	LM	SUERC-63573
133PC	175-176	Mono. NPS	11200 $\pm$ 30	12690 $\pm$ 90	12440 $\pm$ 150	11655 $\pm$ 250	LM	441865
133PC	375-376*	Mixed benthic forams	15270 $\pm$ 45	18070 $\pm$ 170	17750 $\pm$ 175	17250 $\pm$ 195	SMC	SUERC-67947
133PC	433-438	Mono. NPS	14355 $\pm$ 40	16915 $\pm$ 220	16455 $\pm$ 210	15930 $\pm$ 175	LM	SUERC-67948
133PC	583-588	Mono. NPS	15050 $\pm$ 50	17825 $\pm$ 175	17465 $\pm$ 195	16885 $\pm$ 240	LM	450231

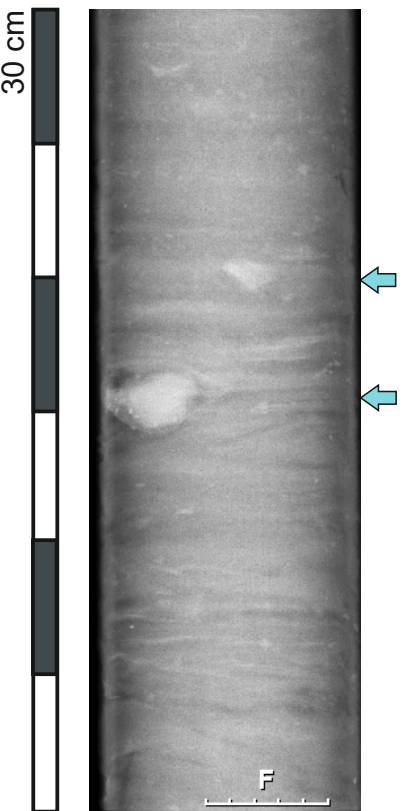






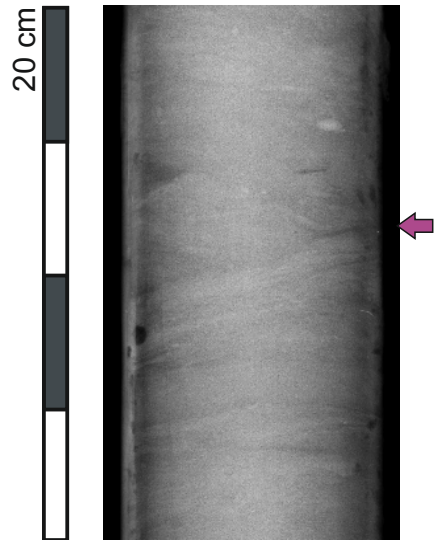
Laminated mud  
rich in IRD

JC106-134PC



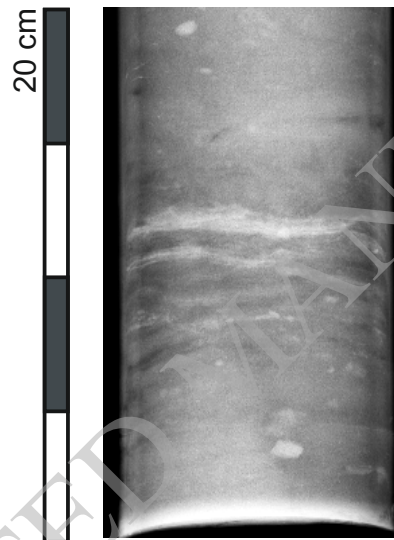
Chaotic  
mud

JC106-134PC



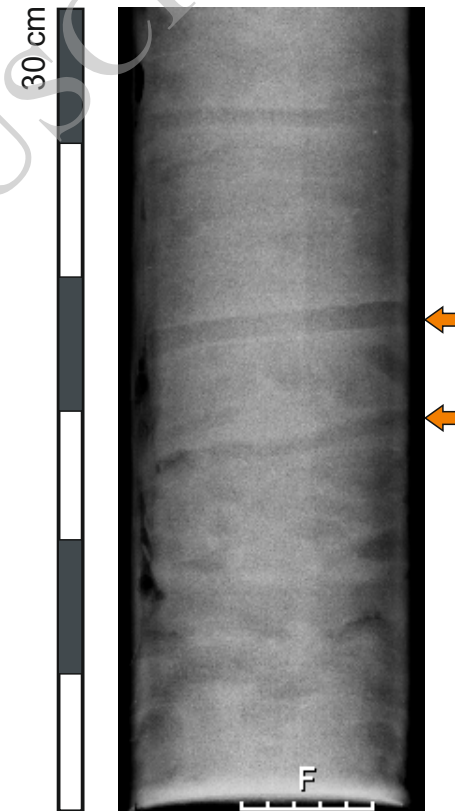
Laminated sand  
to mud couplet

JC106-128PC



Extensively  
bioturbated mud

JC106-133PC



Foraminiferal-  
bearing mud

JC106-128PC

